The bakers's yeast Msh4-Msh5 associates with double-strand break hotspots and chromosome axis during meiosis to promote crossovers

Krishnaprasad G. Nandanan[1*], Ajith V. Pankajam[1*], Sagar Salim[1*], Miki Shinohara[2], Gen Lin[3], Parijat Chakraborty[1], Lars M. Steinmetz[3,4,5], Akira Shinohara[6], Koodali T. Nishant[1,]

[1]School of Biology, Indian Institute of Science Education and Research Thiruvananthapuram, Trivandrum 695016, India

[2]Department of Advanced Bioscience, Kindai University, Nara 631-8505, Japan

[3]Genome Biology Unit, European Molecular Biology Laboratory, Heidelberg 69117, Germany

[4]Department of Genetics, Stanford University, Stanford, CA 94305, USA

[5]Stanford Genome Technology Center, Palo Alto, CA 94304, USA

[6]Institute for Protein Research, Osaka University, Osaka 565-0871, Japan

* Joint first authors

Corresponding author:

Dr. Nishant K.T

School of Biology

Indian Institute of Science Education and Research Thiruvananthapuram

Maruthamala (PO), Vithura, Thiruvananthapuram 695551, India

Telephone: +91-471-2778173, Email: nishantkt@iisertvm.ac.in

Short title: Chromosomal localization of yeast Msh4-Msh5

All raw sequence data for this study are available from the National Centre for Biotechnology Information Sequence Read Archive under accession number SRP129066.

ABSTRACT

Segregation of homologous chromosomes during the first meiotic division requires at least one obligate crossover/exchange event between the homolog pairs. In the baker's yeast *Saccharomyces cerevisiae* and mammals, the mismatch repair-related factors, Msh4-Msh5 and Mlh1-Mlh3 generate the majority of the meiotic crossovers from programmed double-strand breaks (DSBs). To understand the mechanistic role of Msh4-Msh5 in meiotic crossing over, we performed genome-wide ChIP-sequencing and cytological analysis of the Msh5 protein in cells synchronized for meiosis. We observe that Msh5 associates with DSB hotspots, chromosome axis, and centromeres. We found that the initial recruitment of Msh4-Msh5 occurs following DSB resection. A two-step Msh5 binding pattern was observed: an early weak binding at DSB hotspots followed by enhanced late binding upon the formation of double Holliday junction structures. Msh5 association with the chromosome axis is Red1 dependent, while Msh5 association with the DSB hotspots and axis is dependent on DSB formation by Spo11. Msh5 binding was enhanced at strong DSB hotspots consistent with a role for DSB frequency in promoting Msh5 binding. These data on the *in vivo* localization of Msh5 during meiosis have implications for how Msh4-Msh5 may work with other crossover and synapsis promoting factors to ensure Holliday junction resolution at the chromosome axis.

46 **AUTHOR SUMMARY**

47 During meiosis, crossovers facilitate physical linkages between homologous
48 chromosomes that ensure their accurate segregation. Meiotic crossovers are initiated from
49 programmed DNA double-strand breaks (DSBs). In the baker's yeast and mammals, DSBs are
50 repaired into crossovers primarily through a pathway involving the highly conserved mismatch
51 repair related Msh4-Msh5 complex along with other crossover promoting factors. *In vitro* and
52 physical studies suggest that the Msh4-Msh5 heterodimer facilitates meiotic crossover formation
53 by stabilizing Holliday junctions. We investigated the genome-wide *in vivo* binding sites of
54 Msh5 during meiotic progression. Msh5 was enriched at DSB hotspots, chromosome axis, and
55 centromere sites. Our results suggest Msh5 associates with both DSB sites on the chromosomal
56 loops and with the chromosome axis to promote crossover formation. These results on the *in*
57 *vivo* dynamic localization of the Msh5 protein provide novel insights into how the Msh4-Msh5
58 complex may work with other crossover and synapsis promoting factors to facilitate crossover
59 formation.

60

61

62

63

64

65

66

67

68 **INTRODUCTION**

69 During meiosis in baker's yeast, crossover formation is initiated from programmed
70 DNA double-strand breaks (DSBs) made by Spo11 and accessory proteins [1-3]. Crossovers,
71 together with sister chromatid cohesion, facilitate homologous chromosome segregation by
72 physically linking the homologs and properly orienting them towards opposite poles of the
73 bipolar spindle [4]. A fraction of the DSBs are repaired using the homologous chromosome as a
74 template to generate crossovers, and the rest are repaired either as noncrossovers using the
75 homolog or using the sister chromatid as template [5, 6]. In humans, failure to obtain at least one
76 crossover per homolog pair can lead to aneuploid gametes that result in birth defects in offspring
77 [7].

78 Meiotically induced DSBs are non-randomly positioned in the genome. Multiple
79 factors, including open chromatin structure, the presence of certain histone modifications, and
80 the binding of sequence-specific transcription factors are known to influence the spatial
81 positioning of DSBs [8, 9]. In *S. cerevisiae*, during meiotic prophase, chromosomes are
82 organized into a series of loops that are tethered at the base by proteinaceous axial elements
83 mainly consisting of proteins Red1 and Hop1 and the meiotic cohesion complex containing Rec8
84 [10-15]. The chromatin loops originating from the cohesin enriched axis regions have conserved
85 density (~20 loops per micron of axis length) across organisms [12, 16]. In *S. cerevisiae* loops
86 are between 0.2 to 0.6 um long (from axis to the distal-most sequence in the loop) containing up
87 to 20 kb of DNA [12, 17]. Within the Red1-rich axis domains, DSBs are made at a distance
88 from the axis on the loops [16]. But DSB-promoting proteins are associated with axis regions as
89 well, indicating that DSB formation takes place in the context of the loop-axis structure of the
90 chromosomes [18, 19]. Based on these findings, it has been hypothesized that chromosomal

91 loops are recruited to the proximity of the axis for DSB formation and repair [20-22]. This
92 allows events at both loop and axis levels to be functionally linked and coordinated [16, 17].
93 The chromosome axis proteins influence the formation of DSBs, promote interhomolog bias, and
94 facilitate the biased resolution of double Holliday Junction (dHJ) intermediates [23].

95 In *S. cerevisiae*, the major pathway for the repair of DSBs as crossovers is mediated by
96 the ZMM group of proteins (Zip1, Zip2, Zip3, Zip4, Mer3, Msh4, Msh5, and Spo16) along with
97 MutLγ (Mlh1 and Mlh3), Exo1, and the STR complex (Sgs1, Rmi1, Top3) to facilitate the
98 formation of ~80% of crossovers [24-28]. The ZMM-mediated crossovers show interference and
99 are called class I crossovers. A minor set of crossovers that are interference-independent (class
100 II) are produced by a pathway involving the Mms4-Mus81 protein complex, which can directly
101 act on D-loops or Holliday junction intermediates to form crossovers [29, 30].

102 The Msh4 and Msh5 proteins are homologs of the bacterial MutS family of mismatch
103 repair proteins with no known function in mismatch repair [31]. The Msh4 and Msh5 proteins
104 function together as a heterodimer [32]. In *S. cerevisiae*, both *msh4Δ* and *msh5Δ* mutants show a
105 substantial reduction in meiotic viability along with crossover defects and Meiosis I non-
106 disjunction [30, 33]. *In vitro* biochemical studies using purified human Msh4 and Msh5 show
107 that these proteins bind to Holliday junction substrates and stabilize them [34]. Similarly, *in*
108 *vitro* biochemical and physical studies in *S. cerevisiae* show that Msh4-Msh5 stabilizes 3'-
109 overhangs, single-end invasion (SEI) intermediates, and Holiday junctions [24, 35]. Further,
110 Msh4 has a degron, which is phosphorylated by cdc7 kinase to stabilize the Msh4-Msh5 complex
111 and promote a crossover outcome [36]. Recent genetic, biochemical, and physical studies
112 suggest that the Msh4-Msh5 complex acts in the same pathway as the Mlh1-Mlh3 complex,
113 Exo1, and PCNA to process inter homolog joint molecule structures into crossover products [27,

114 37-41]. The Msh4-Msh5 complex has a role in directing the activity of the Mlh1-Mlh3
115 endonuclease to generate crossovers from double Holliday junctions [27, 40, 41]. In mammals,
116 mutation of *Msh4* or *Msh5* results in sterility [42, 43]. Cell biological observations in the mouse
117 show a large number of Msh4/Msh5 foci (~ 140 per nucleus) during an early stage (Zygotene) of
118 meiosis [44]. As meiosis progresses, the number of Msh4/Msh5 foci decreases, and at mid
119 pachytene stage, they are present at almost twice the number of actual crossing over sites. At
120 this stage, almost half of the Msh4/Msh5 foci co-localize with Mlh1/Mlh3 foci, which are
121 considered to be the sites for crossover [42, 45, 46]. Although few aspects of Msh4-Msh5
122 function are known, an understanding of the *in vivo* DNA binding sites, recombination substrates
123 and localization with reference to the chromosomal organization during meiosis is lacking.

124 We analyzed the chromosome-binding properties of the Msh4-Msh5 complex using
125 chromatin immunoprecipitation and sequencing (ChIP-Seq), ChIP-qPCR, and cytology in
126 synchronized meiotic time courses. We found that Msh5 is specifically enriched at DSB
127 hotspots [18]. Additionally, Msh5 binding is also observed at the chromosome axis and
128 centromeres. Msh5 binding at DSB hotspots and chromosome axis is disrupted in *spo11*
129 mutants, while axis association is disrupted in *red1*Δ. Msh5-binding sites on chromosomes are
130 similar to Zip3 and the ZZS complex (Zip2, Zip4, Spo16) [47-49]. Further Msh5 binding at
131 chromosome axis and centromeres also suggest crossover-independent functions related to
132 chromosome synapsis. Our observations suggest that Msh5 is enriched at strong DSB hotspots
133 that have high DSB frequency. These results shed novel insights into the role of the
134 chromosome loop-axis structure on the assembly of the Msh4-Msh5 complex during meiosis.
135 They are also useful for developing models for how Msh4-Msh5 may coordinate both crossover
136 and synapsis events.

137 # RESULTS

138 **Genome-wide analysis shows Msh5 binding at DSB hotspots, chromosome axis, and**
139 **centromeres**

140 Msh5 protein expression starts at 2h after induction of meiosis and remains till 8h with
141 peak expression at 5h (**Fig 1A**). To characterize the dynamic binding of Msh5 during the
142 different stages of meiosis, we performed ChIP-Seq from meiotic extracts using an anti-Msh5
143 antibody. The Msh5 antibody was generated in rabbit and is polyclonal. 5ul Msh5 serum was
144 used for each ChIP-Seq experiment. No Msh5 protein band was observed in the *msh5Δ* lysate or
145 eluate fractions, showing the specificity of the antibody (**Fig 1B**). Msh5 ChIP-Seq was
146 performed in quadruplicate at six-time points, from 2h to 7h at one-hour intervals. The Msh5
147 binding data from the four replicates (a-d) at the 5h time point was highly reproducible (r = 0.72-
148 0.93) (**S1 A-F Fig**). Msh5 ChIP-Seq data from the four replicates were normalized using input,
149 and genome-wide plots were generated to detect Msh5-peak positions along the chromosomes
150 (Materials and Methods). A total of 3397 Msh5 peaks were observed from all four replicates
151 (with $p < 10^{-5}$, see Materials and Methods) at 5h post entry into meiosis (**S1 Table**). Previous
152 studies of the ZMM proteins have shown that Zip3, as well as the ZZS complex (Zip2, Zip4,
153 Spo16) mostly associate with DSB hotspots and show weak and transient association with the
154 chromosome axis [47]. Msh5 (and Msh4) functions as a distinct complex from Zip3 and ZZS
155 [47, 50]. We therefore analyzed Msh5 binding with reference to DSB hotspots [18] and
156 chromosome axis sites [15]. Representative Msh5 binding plot from all four replicates for
157 chromosome III at 3h, 4h, and 5h, shows Msh5 associates with DSB hotspots, chromosome axis
158 sites, and also centromere position while being depleted from DSB coldspots (**S2A Fig**). The
159 Msh5 binding sites were validated using qPCR. Binding of Msh5 at three representative DSB

160 hotspots (*BUD23*, *ECM3*, *CCT6*), three axis sites (*Axis I*, *Axis II* and *Axis III*), two centromere
161 locations (*CENI, CENIII*) and one coldspot (*YCRO93W*) were analyzed from the same time
162 course in one of the replicates (d). The qPCR results confirm that Msh5 is specifically enriched
163 at DSB hotspots, chromosome axis and centromeres relative to DSB cold spots (**Fig 1C** and **S2B**
164 **Fig**). The qPCR data was further used to scale the corresponding Msh5 ChIP-Seq replicate (d)
165 (Materials and Methods) (**S3A Fig**). From the scaled Msh5 ChIP-Seq data, maximum Msh5
166 binding is observed between 3-5h relative to other time points (6h, 7h) across all chromosomal
167 locations consistent with Msh5 expression (**Fig 2A**). The scaled Msh5 ChIP-Seq plot is shown
168 for chromosome III as a representative example (**Fig 2B**). We observed that Msh5 binds weakly
169 to DSB hotspots at an early stage (3h) after induction of meiosis (**Fig 2B**). At later stages of
170 meiotic progression (4h and 5h) maximum Msh5 binding was seen at DSB hotspots (**Fig 2B**).
171 Statistical analysis of the scaled Msh5 coverage data at DSB hotspots (non-overlapping with
172 Red1 sites) showed binding differences at 3h, 4h, and 5h are significantly different (t-test) (**Fig**
173 **2C**). Further, maximum Msh5 binding at DSB hotspots is seen at 4h -5h (**Fig 2C**). Msh5 peaks
174 from all four replicates associated with DSB hotspots at 5h showed a median width of 0.5kb
175 (mean 0.9kb) (**Fig 2D**). This result suggests that Msh5 binding at DSB hotspots is confined to
176 the width of the heteroduplex region during DSB repair (1-2 kb) [51].

177 We analyzed binding data of Msh5 in meiotic time courses at axis sites (Red1 binding
178 regions) [15]. Representative plot for chromosome III shows the overlap of Msh5, and Red1
179 reads from 3h to 5h (**Fig 2B**). Msh5 binding at Red1 sites (non-overlapping with Spo11 sites)
180 from 3h to 5h is significantly different between the time points with maximum binding at 5h (**Fig**
181 **3A**). These observations suggest Msh5 binds to both DSB hotspots and axis from 3h to 5h.

182 Together, these observations support Msh5 association with both DSB sites at chromosomal
183 loops and axis regions.

184 In addition to DSB hotspots and axis, ChIP-qPCR and ChIP-Seq analysis also showed
185 binding of Msh5 at representative centromere regions **(Fig 1C, 2B, S2A, B).** Also, earlier
186 binding of Msh5 at centromeres (e.g. at 3h) is observed compared to the DSB hotspots and axis
187 sites (**Fig 3B**). Individual chromosome plots show Msh5 associates with centromeres on all
188 chromosomes **(S4 Fig).** Association with centromeres is also observed for other ZMM proteins
189 like Zip3 [48].

190 qPCR analysis showed no Msh5 enrichment in *msh5*Δ mutant at DSB hotspots relative
191 to the coldspot (**S5A Fig**). Axis and centromeres (which show reduced Msh5 enrichment
192 compared to DSB hotspots) showed background levels of Msh5 binding in *msh5Δ*. qPCR
193 analysis also showed no enrichment of Msh5 in *msh4Δ* mutant at DSB hotspots (**S5B Fig**).
194 However, weak Msh5 binding is observed at axis and centromere in *msh4Δ* (**S5B Fig**) consistent
195 with earlier cytological observations showing residual Msh5 signals in *msh4Δ* [25]. Therefore,
196 Msh4-Msh5 complex formation is required for normal Msh5 enrichment at DSB hotspots, axis,
197 and centromeres.

198 Since other ZMM proteins (Zip2, Zip3, Zip4, Spo16) have been observed to associate
199 with the centromere, chromosome axis and DSB hotspots in ChIP-array and ChIP-Seq studies
200 [47, 48], we re-analyzed Zip3 binding to facilitate comparison with the Msh5 binding data in the
201 same strain background and experimental conditions. We used a Zip3 construct C-terminally
202 tagged with three copies of the FLAG epitope [48]. The diploid strain expressing *ZIP3-His6-*
203 *FLAG3* allele showed a spore viability of 97% (40 tetrads dissected), as reported previously
204 [48]. Zip3 expression was detected using an anti-FLAG antibody (mouse) from 2h after

205 induction of meiosis till 8h with peak expression at 5h (**S6A Fig**). Zip3 ChIP from meiotic
206 extracts was performed at 3h, 4h, and 5h using an anti-FLAG antibody. No Zip3 protein band
207 was observed in the untagged wild-type lysate or eluate fractions showing the specificity of the
208 antibody (**S6B Fig**). Zip3 ChIP-Seq was performed once for 3h time point and in duplicates for
209 4h and 5h time points. Representative binding of Zip3 on chromosome III is shown in **S6C Fig**.
210 Like Msh5, Zip3 shows binding to DSB hotspots, chromosome axis sites, centromere and is
211 absent from DSB cold spots (**S6C Fig**) as observed previously [47, 48].
212

213 **Msh5 binding at DSB hotspots is stimulated by DSB repair intermediates**

214 We performed cytology in meiotic time courses with the Msh5 antibody in several
215 mutant backgrounds that affect DSB formation and processing to determine genetic requirements
216 for Msh4-Msh5 localization at DSB hotspots. In wild-type cells, we observed a peak in the
217 average number of Msh5 foci/cell (48 ± 6.5) at 5h (**Fig 4A, C**). Previous studies have also
218 observed a similar number of Msh5 foci in wild type [36, 49]. In a *spo11*Δ mutant where DSBs
219 are not formed, cytological observations showed no Msh5 foci (**Fig 4B, C**) at any of the time
220 points in meiosis. Consistent with previous studies, these observations suggest that Msh5
221 binding to the DNA is dependent on DSB formation [49]. We asked if DSB formation and
222 resection are sufficient for the binding of Msh5 protein. In *dmc1*Δ mutant, cells arrest after DSB
223 formation and resection [52]. The joint molecule formation is blocked completely in *dmc1Δ*
224 mutant [53]. These cells cannot repair DSBs because of the loss of strand exchange activity [52,
225 54]. Compared to wild type (48 ± 6.5 Msh5 foci), on average 22 ± 3.8 Msh5 foci were observed
226 at 5h in a *dmc1*Δ mutant **(Fig 4A-C).** These results indicate that an event prior to the Dmc1
227 function, such as DSB resection, promotes Msh5 binding. Such an observation is also consistent

228 with *in vitro* data showing Msh4-Msh5 can bind to 3' overhangs [35]. It has been shown that in
229 the *dmc1*Δ mutant, the DSBs appear at the normal time but persist longer, and the cells get
230 arrested at this stage [52]. The reduced number of Msh5 foci (22 ± 3.8) in *dmc1*Δ mutant
231 compared to wild type (48 ± 6.5, $p < 0.001$) is therefore not due to reduced DSBs. Instead, this
232 observation suggests that even though resected DSBs can recruit Msh5, the binding efficiency to
233 resected DSB structures is reduced. Dmc1-dependent strand invasion steps, therefore, promote
234 stable binding of Msh5.

235 We tested Msh5 binding in a *rad52*Δ mutant where cells efficiently proceed to strand
236 invasion and make wild-type level of SEI intermediates, but dHJ formation is significantly
237 reduced [55, 56]. The timing and frequency of DSBs are similar in *rad52*Δ and wild type [55].
238 We observed an average of 31 ± 6 Msh5 foci at 5h in the *rad52*Δ mutant (**Fig 4B, C**), which is
239 less compared to wild type ($p < 0.001$). Since SEIs are similar in *rad52*Δ and wild type, but SEI
240 + dHJs are about two times more in wild type, the number of Msh5 foci in *rad52*Δ (31 ± 6) and
241 wild type (48 ± 6.5) suggests that SEI intermediates are efficient for recruiting Msh4-Msh5.
242 Taken together with previous observations of lack of Msh5 foci in *spo11*Δ and *rad50S* mutants
243 [49], our results in *dmc1Δ* and *rad52Δ* suggest in *S. cerevisiae* Msh4-Msh5 recruitment *in vivo*
244 happens after DSB resection, which is consistent with *in vitro* biochemical data showing binding
245 of *S. cerevisiae* and human Msh4-Msh5 at SEI structures [34, 35].

246 Next, we asked if dHJs stimulate maximum Msh5 binding using the *ndt80*Δ mutant that
247 accumulates joint molecules, but the dHJs are not resolved [5]. An average of 47 ± 6.4 Msh5
248 foci is observed at 5h in *ndt80*Δ mutant which is similar to the maximum number of Msh5 foci
249 seen in the wild type at 5h ($p = 0.44$, **Fig 4A-C**) indicating that the SEI and dHJ structures
250 together facilitate maximum binding of the Msh4-Msh5 complex to the DNA. These results

251 suggest that even though resected DSBs can initiate binding of the Msh4-Msh5 complex,
252 maximum binding is achieved with joint molecule structures comprising SEIs and dHJs (see
253 discussion). In addition, the average Msh5 foci count (51) at 6h in *ndt80Δ* is higher than wild
254 type (40.7) due to the accumulated levels of SEIs and dHJ structures. Msh5 aggregates were
255 observed in all the above mutants (*spo11Δ*, *dmc1Δ*, *rad52Δ*, *ndt80Δ*) and is quantified in **S7 Fig.**
256

257 **Msh5 binding depends on DSB strength**

258 We tested the correlation between DSB frequency and Msh5 association with
259 chromosomes. ChIP-qPCR analysis corroborated cytological observations of the absence of
260 Msh5 binding in *spo11*Δ. ChIP-qPCR analysis showed no enrichment of Msh5 at DSB hotspots
261 and axis relative to DSB coldspot (**S5C Fig**). But early binding (3h) at centromeres was
262 observed, suggesting Msh5 enrichment at DSB hotspots and chromosome axis is dependent on
263 DSB formation (**S5C Fig**). In budding yeast 3600 DSB hotspots have been identified in high
264 resolution [18]. These DSB hotspot positions (Spo11 cutting sites) were obtained from Pan et
265 al., 2011[18]. We defined DSB hotspots that show Msh5 peak at 5h time point ($p < 10^{-5}$) in at
266 least one of the four replicates as Msh5 enriched DSB hotspots. DSB hotspots that did not show
267 Msh5 peak (or $p > 10^{-5}$) in any of the four replicates were defined as Msh5 depleted DSB
268 hotspots. Our analysis suggests that about half of the 3600 identified DSB hotspots (1734/3600)
269 are enriched for Msh5 protein (**S2 Table**). We observed that Msh5 enriched DSB hotspots
270 showed higher Spo11 oligo counts (**Fig 5A, S2 Table**). Among the top 10% of DSB hotspots
271 (based on Spo11 oligo counts,[18]), 96% were Msh5 enriched DSB hotspots and 4% were Msh5
272 depleted DSB hotspots ($p < 0.01$) (**S2 Table**). Among the bottom 10% of DSB hotspots, 27%
273 were Msh5 enriched DSB hotspots, and 73% were Msh5 depleted DSB hotspots ($p <0.01$). This

274 observation suggests Msh5 is easily detected at active DSB hotspots as more cells in the
275 population would have the break.

276 Small chromosomes have a higher density of crossovers than long chromosomes, which
277 is correlated with a higher Spo11 oligo density on the smaller chromosomes [18, **Fig 5B**]. Msh5
278 read density (reads / Kb) analyzed from all four replicates was negatively correlated with
279 chromosome size (r = -0.72; p = 0.0016) consistent with more crossovers / kb and higher DSB
280 activity on smaller chromosomes (**Fig 5C**). These observations also support Msh5 enrichment is
281 dependent on DSB activity. Zip3 read density showed weaker correlation with chromosome size
282 (r = -0.56, p = 0.02) (**Fig 5C**). A recent study shows that the three smallest chromosomes (I, III,
283 and VI) have unusually high DSB density due to distinct regulation of DSB formation that
284 ensures their accurate segregation [57]. Although Spo11 oligo density (and crossover density) is
285 negatively correlated with chromosome size even after excluding the three smallest
286 chromosomes [57], Msh5 read density showed weak negative correlation (r = -0.6, p = 0.03),
287 while Zip3 read density (r = -0.18, p = 0.55) was uncorrelated with chromosome size (**Fig 5D**).
288

289 **Msh5 binding to the chromosome axis is disrupted in *red1*Δ mutant**

290 Since Msh5 binding is positively correlated with the Red1 axis associated sites, we
291 tested whether loading of Msh5 is dependent on the Red1 protein. Red1, an axial element
292 protein, is essential for normal DSB formation by recruiting DSB factors to the axis, synapsis,
293 and for promoting interhomolog DSB repair through its role in meiotic checkpoint signaling [19,
294 58-61]. Cytological observations showed that the number of Msh5 foci in *red1*Δ was
295 significantly less than the number of Msh5 foci in wild type at all time points (3h, 4h, 5h, 6h) in
296 meiotic time courses with no overlap in the standard deviation (**Fig 6A, S1 Data**). At 5h an

297 average of 16 ± 5.3 Msh5 foci is observed in *red1*Δ compared to 48 ± 6.5 foci ($p < 0.001$) in wild
298 type (**Fig 6A**). Since the number of Msh5 foci is less compared to wild type, we also examined
299 the DSB frequency using Rad51 foci counts. We observed an average of 20 ± 4.3 Rad51 foci at
300 a three-hour time point when the numbers of DSBs are at peak level (**Fig 6B**). Previous studies
301 have also shown that DSBs are decreased in *red1Δ* mutant [60]. The average number of Rad51
302 foci in *red1*Δ is significantly less compared to the number of Rad51 foci in wild type at 3h (49 ±
303 15, $p < 0.001$) [58]. The reduced number of Msh5 foci in *red1*Δ is most likely due to overall
304 reduction in DSB levels, and since DSB repair is mostly off the sister chromatid [61-63].
305 ChIP-qPCR analysis showed no enrichment of Msh5 at representative axis sites relative
306 to the DSB coldspot in *red1*Δ at an early time point (3h) (**S5D Fig**). Msh5 association was
307 maintained at representative DSB hotspots and centromeres (**S5D Fig**). ChIP-Seq analysis of
308 Msh5 protein in the *red1*Δ mutant scaled with qPCR data (at 5h, **S3B Fig**) confirmed Msh5 is
309 depleted at axis sites and maintained at DSB hotspots and centromere sites (**Fig 6C**). Overall
310 these observations suggest that Red1 is essential for Msh5 binding at axis regions but not at DSB
311 sites and centromere regions.
312

313 **DISCUSSION**

314 Previous studies using cytological, biochemical, and physical approaches in various
315 organisms have given insights into the timing of Msh4/Msh5 action, and it's *in vitro* DNA
316 binding properties. Purified human Msh4-Msh5 has a high affinity towards SEI and dHJs [34],
317 and the *S. cerevisiae* Msh4-Msh5 has also been shown to bind 3' overhangs, pro-Holliday
318 junctions and Holliday junction structures [34, 35]. But the genome-wide dynamic localization
319 of the Msh4-Msh5 complex with reference to its *in vivo* binding sites, meiotic chromosomal

320 organization, and mutations in other meiotic recombination genes is not well understood. The
321 current model of meiotic recombination based on *in vitro* biochemical analysis suggests Msh5
322 associates with 3' overhangs, SEI, and dHJs. We demonstrate that *in vivo,* Msh5 associates with
323 DSB hotspots, chromosome axis, and centromere sites. Recruitment of Msh5 to DSB hotspots
324 and chromosome axis requires DSB formation and is observed as early as the stage of DSB
325 resection (**Fig 4**).

326 Msh5 foci in *dmc1*Δ mutants, where DSBs are formed and resected but cannot undergo
327 strand invasion is consistent with *in vitro* studies (**Fig 4**) [35]. It is possible that Msh5 binding in
328 *dmc1Δ* may reflect aberrant binding due to the hyperresected DSBs. Further studies are required
329 to explain whether this binding has any functional relevance or is just related to its recruitment.
330 Although resected DSBs are sufficient for the initial recruitment of Msh5, the optimal binding of
331 Msh5 requires the formation of dHJs (**Fig 4**). ChIP-Seq results also suggest weak binding of
332 Msh5 at DSB hotspots at the early stages of meiosis (3h) and maximal binding at DSB hotspots
333 around 4-5h that corresponds to joint molecule formation. These results, along with previous
334 studies showing Msh2 associates with DSBs *in vivo* [64] suggest a general property of MSH
335 proteins to bind DNA that facilitates specific binding to their major substrates.

336 Msh5 binding is observed at chromosome axis sites from 3 to 5h with maximum
337 binding at 5h. This observation supports previous cytological studies that show localization of
338 Msh5 and Msh4 at the chromosome axis [50, 65]. The observation that Msh5 associates with
339 both DSB and chromosome axis sites suggest that Msh5 may participate in both the processing
340 of recombination intermediates and the assembly of the synaptonemal complex like some of the
341 other ZMM proteins [66]. Thus it may have a role in crossover formation and synapsis. It is

342 also possible that Msh5 binding to the axis is indirect via interactions with axis proteins. A
343 recent study has implicated interactions between Msh5 and Red1 [47].

344 The Msh5 protein also shows binding to centromere sites on all chromosomes. Other
345 ZMM proteins like Zip2, Zip3, Zip4, and Spo16 also show centromere localization. It is
346 suggested that Zip1, Zip2, Zip3, and Spo16 binding to centromeres promotes synapsis initiation
347 from centromeres, besides crossover sites [67]. It is also suggested that Zip1 localization to
348 centromere facilitates non-exchange chromosome segregation. Just as Msh5 association with
349 chromosome axis, may facilitate synapsis, it is possible that Msh5 localization to centromeres
350 may also facilitate synapsis initiation, especially as it is observed even in *spo11*Δ mutant at early
351 time points (**S5C Fig**). Alternatively, it is possible that Msh5 binding at centromere may reflect
352 a docking site for the protein or is indirect through interactions with other ZMM or centromeric
353 proteins.

354 Cytological and ChIP-array studies also show that some of the ZMM proteins Zip1 and
355 Zip3 associate with the chromosome axis [19, 48]. A recent study by De Muyt et al. 2018 [47]
356 suggests that ZZS (Zip2, Zip4, Spo16) and Zip3 show strong association with DSB hotspots and
357 weak and transient association with chromosome axis. Similar to Zip3 and the ZZS complex,
358 which associate with the centromere, chromosome axis, and DSB hotspots in a dynamic manner
359 [48], Msh5 associates with centromeres, chromosome axis and DSB hotspots (**Fig 1C**, **Fig 2B**).
360 Further, Msh5 loading is dependent on Zip3 protein [25], and Zip3 and Msh4 foci co-localize
361 cytologicaly. This is supported by our observation that Zip3 and Msh5 occupy similar
362 chromosomal features (**S6C Fig**, **Fig 1C**, **Fig 2B**). Although there are similarities between Zip3
363 and Msh5 binding sites, Msh5 binding is also stimulated by DSB frequency (**Fig 5**, **S2 Table**).
364 These observations support a direct role for Msh5 in the mechanism of crossover formation.

365 **Model for Msh4-Msh5 function in crossing over**

366 Chromosome domains with high DSB activity are enriched for Red1 at the axis. But within the
367 Red1 enriched domain, there is a negative correlation between Spo11/Dmc1 and Red1 sites since
368 DSBs occur on the loop while Red1 sites are on the axis [16, 19]. We observed that about half of
369 all DSB hotspots are detectably enriched for Msh5. The Msh5 localization supports the model
370 that recombination occurs in sequences that are at a distance from the base of the chromosome
371 loops [16]. The Msh5 binding data also suggests that within axis protein-enriched regions, the
372 Msh4-Msh5 complex binds to the DSB hotspots that are known to occur at a distance from the
373 axis. We also observe Msh5 association with the chromosome axis from 3h to 5h time point.
374 The axial association is absent in a *spo11*Δ mutant (**S5C Fig**), which suggests, DSBs may
375 promote Msh5 assembly on the chromosome axis. At 4-5h, Msh5 binds both DSB and axis
376 optimally, which may facilitate communication between DSB sites and axis through Msh5 for
377 crossover formation. Msh5 may be part of the recombinosome for loops tethering to the axis.
378 Based on our observations that the Msh4-Msh5 complex binds to DSB hotspots on chromosomal
379 loops and also on the axis, a model for how Msh4-Msh5 may work in crossover formation is
380 shown in **Fig 7**.

381 Similar to the loop – axis interaction required for meiotic DSB formation, we speculate a
382 loop-axis interaction model for crossover formation. Specifically, Msh4-Msh5 association on
383 chromosome loops and axis following DSB formation may facilitate the recruitment of the
384 Mlh1-Mlh3 complex at these locations. Recent *in vitro* studies suggest that the Mlh1-Mlh3
385 complex forms unidirectional polymers on DNA and that polymerization is essential for its
386 nicking activity [27, 68]. Since Msh4-Msh5 encircles both interacting duplexes during joint
387 molecule formation, it could direct polymerization on both duplex arms. The Mlh1-Mlh3

388 complex could polymerize directionally from the loop associated Msh4-Msh5 complex towards
389 the axis. Since the Msh4-Msh5 complex is also associated with the axis, it could facilitate loop-
390 axis interaction for crossover formation near the axis by Mlh1-Mlh3. Also, human Msh4-Msh5
391 is known to stimulate human Mlh1-Mlh3 endonuclease activity [40, 41]. Crossover formation at
392 the axis can facilitate long-range interference through the dissipation of mechanical stress along
393 the axis [69, 70]. This axis-loop interaction during crossover formation may also be required to
394 convert crossovers into chiasma. In conclusion, these data shed novel insights into the *in vivo*
395 assembly and functions of the Msh4-Msh5 complex in relation to meiotic chromosome
396 organization and DSB activity.
397

398 **MATERIALS AND METHODS**

399 **Yeast strains and media**

400 Yeast strains used in this study are derivatives of *S. cerevisiae* SK1 strain and are listed in
401 the **S3 Table.** Yeast strains were grown on either yeast extract–peptone–dextrose (YPD) or
402 synthetic complete media at 30^0 [71-73]. Sporulation medium was prepared as described in
403 Argueso et al. (2004) [30]. Mutants were generated by direct transformation using standard
404 techniques [74]. When required, the drugs geneticin (Invitrogen), nourseothricin (Werner
405 BioAgents,Germany), and hygromycin (Sigma) were added to the media at prescribed
406 concentrations [75].
407

408 **Meiotic synchronization**

409 Meiotic synchronization was performed using SPS method as described [76]. In short,
410 diploid colonies were inoculated in 5 ml YPD medium and grown for 24h at 30^0 C to reach

411 saturation. From the saturated YPD culture ~ 5 x 10^6 cells/ml were inoculated to liquid SPS
412 (0.5% yeast extract, 1% peptone, and 0.67% yeast nitrogen base without amino acids, 1%
413 potassium acetate, 0.05M potassium biphthalate, and pH 5.5) medium and grown for 7h at 30^0 C.
414 This culture was used to inoculate 500 ml of liquid SPS at cell density ~ 3 x 10^5 cells/ml and
415 grown for 12-16h at 30^0 C until the cell density reached ~4 x 10^7 cells/ml. Cells were collected
416 by centrifugation, washed twice with 1% potassium acetate and re-suspended in 400 ml of
417 sporulation (2% Potassium Acetate) medium at cell density ~ 4 x 10^7 cells / ml and incubated at
418 30^0 C with shaking. Meiotic progression was monitored by examining the nuclear divisions
419 using DAPI staining.
420

421 **Chromatin Immunoprecipitation**

422 Msh5 ChIP was performed as described in [19, 76, 77] with minor modifications, using
423 native Msh5 antibody and Protein A Sepharose beads (GE Healthcare). Briefly, from a
424 synchronous meiotic culture, 50 ml of samples were collected at various time points (as
425 described in the results) and crosslinked using formaldehyde. Cells were lysed using
426 Beadbeater. The cell extract was sonicated using Bioruptor (Diagenode) and the debris were
427 removed by centrifugation. 50 ul of Protein A sepharose beads were used to preclear the cell
428 lysate from each sample. To the pre-cleared lysate, Msh5 antibody and Protein A sepharose
429 beads blocked with BSA was added. After incubation, lysate was removed by centrifugation and
430 beads were washed to remove non-specific binding. The immunoprecipitated material was
431 eluted from the beads and decrosslinked along with RNAse A treatment. The DNA was purified
432 following Proteinase K treatment using QIAGEN PCR purification kit. Lysate samples were
433 collected before and after the immunoprecipitation and after elution to check for IP efficiency by

434 Western blotting. Zip3 ChIP was performed using anti-FLAG antibody and Protein G
435 Dynabeads (Life technologies). For Msh5 western blot, anti-Msh5 antibody was used at 1:4000
436 dilution, and anti-rabbit HRP secondary antibody was used at 1:10000 dilution. For Zip3
437 western blot, anti-FLAG antibody was used at 1:4000 dilution, and anti-mouse HRP secondary
438 antibody was used at 1:10000 dilution. Anti-PGK1 antibody was used at 1:30000 dilution, and
439 anti-mouse HRP secondary antibody was used at 1:40000 dilution. The immunoprecipitated
440 DNA was used for sequencing as well as qPCR. For wild type, four ChIP samples were
441 sequenced for each time point (2-7h). For the *red1*Δ mutant, three ChIP samples were sequenced
442 at the indicated time points. The DNA fragments were sequenced on Illumina HiSeq 2500/4000
443 platform at Fasteris, Switzerland. qPCR was performed on a fraction of the DNA sample used
444 for ChIP-Seq for wild type and mutants. The DNA enrichment of the ChIP samples were
445 calculated with respect to the input for wild type and mutants at each time point from three
446 technical replicates.
447
448 **Cytology**
449 Yeast chromosome spreads were prepared as described [25, 56] and stained with anti-
450 Msh5 and anti-Rad51 antibody (Rabbit polyclonal antibody from Akira Shinohara) at 1: 500
451 dilution followed by anti-Rabbit TRITC conjugated secondary antibody (Jackson
452 ImmunoResearch) at 1: 1500 dilution. Immunofluorescence images were captured using a 63x
453 oil immersion objective on a Leica SP5 confocal microscope. For each time point,
454 approximately 50 images were analyzed from two independent experiments. For *spo11Δ*, only
455 30-50 images were analyzed at each time point from a single experiment as previous studies
456 show the absence of Msh5 foci in *spo11Δ*. Image analysis and 3D deconvolution were done

457 using Leica Application Suite (LAS) Advanced Fluorescence (AF) Lite 2.8.0 software. All foci
458 counts are shown as mean ± standard deviation.
459
460 **Bioinformatic analysis of Illumina sequence data**
461 Quality and statistics of raw reads were analyzed using FastQC (version 0.11.5).
462 Preprocessing was decided based on the FastQC report summary. Removal of Illumina adapters
463 and trimming of raw sequence reads was done using Trimmomatic (version 0.36). Processed
464 reads (~2-8 Million reads per samples) were aligned to the S288c reference genome (version
465 R64-1-1) using bowtie2 (version 2.3.0) since the SK1 reference genome assembly is incomplete.
466 Previous studies have used both S288c and SK1 as reference genomes and showed that the
467 results are similar [15, 18]. Samples having more than 75% alignment rate and with more than 2
468 million aligned reads were used for the downstream analysis. Statistics of the mapped reads
469 generated from the alignment program were analyzed for uniquely mapped reads as well as for
470 multiple mapped reads. Samples having an alignment rate of less than 30% and less than 0.5
471 million reads were discarded from the analysis. Unmapped reads were analyzed using blast to
472 detect any type of contamination in the sample. After analyzing the alignment statistics,
473 conversion of aligned file format (SAM) to its compressed file format (BAM), indexing and
474 sorting was done using samtools (version 1.3.1). All the downstream analyses were done using
475 R (version 3.3). All raw sequence data for this study are available from the National Centre for
476 Biotechnology Information Sequence Read Archive under accession number SRP129066.
477
478 **Genome-wide profile normalization using NCIS**

479 The S288c reference genome was partitioned into equal-sized bins (200 bp), and reads
480 per bin were calculated from the samples. Reads that are mapped to N locations were assigned a
481 score of 1/N for each read in case of multi-mapped reads. Normalization was performed in order
482 to account for factors affecting the data distribution, such as an error during library preparation,
483 sequencing, and sample preparation. For this study, we performed normalizations with the
484 control sample (Input for Msh5 ChIP and wild type untagged for Zip3 ChIP) using NCIS
485 (Normalization of ChIP-seq). NCIS estimates the fraction of background from the control
486 sample using a data-adaptive length of the window and a data-adaptive threshold assuming that
487 background tends to have lower counts than enriched regions [78]. After normalizing the counts
488 using NCIS, backgrounds were subtracted from their respective control samples and averaged,
489 followed by genome-wide smoothening by ksmooth with a bandwidth of 1 kb.
490

491 **Peak calling using MACS**

492 To identify the Msh5 peaks, only reads that are uniquely aligned were taken into account.
493 MACS (Model-based Analysis for ChIP-Seq) (http://liulab.dfci.harvard.edu/MACS/) [79] was
494 used to identify peaks from the sample. MACS uses a dynamic Poisson distribution to identify
495 local biases in peak detection. Msh5 peaks were called from the pooled set of four replicates.
496 Msh5 peaks with a p-value greater than 10^{-5} were filtered out, and the final set of Msh5 peaks is
497 shown in **S1 Table**. Spo11 DSB hotspots (non-overlapping with Red1 sites) and axis sites
498 (Red1 bound regions non-overlapping with Spo11 sites) were considered as Msh5 enriched if the
499 Msh5 peak showed minimum one base pair overlap with the Spo11 hotspot or the Red1 peak
500 respectively (**S2 Table**). The raw data for calling Red1 peaks were extracted from Sun et al.,
501 2015[15]. Red1 peaks were called following the same criteria described for calling Msh5 peaks,

502 except for p-value, which was set at less than 10^{-15} as per Sun et al., 2015[15]. Zip3 reads were
503 analyzed similarly to Msh5 reads.
504
505 **ChIP-qPCR scaling of Msh5 ChIP-Seq reads**
506 For wild type, one of the four Msh5 Chip-Seq replicates was scaled with the corresponding
507 qPCR data. We performed normalization of the Msh5 Chip-Seq data with respect to its input
508 using NCIS [78]. Linear regression model was generated between the normalized Msh5 Chip-
509 Seq data and the qPCR data [**S3A Fig**] using R scripts provided by Hajime Murakami and Scott
510 Keeney [80]. The linear regression model was used to scale the Msh5 ChIP-Seq data. A similar
511 process was used to scale Msh5 ChIP-Seq reads in the *red1*Δ mutant.
512
513 **Statistical tests**
514 For all count data (foci, box plots) student's t-test was used to test for statistical
515 significance. For all correlation analysis, Pearson's correlation coefficient was used. Numerical
516 data underlying all graphs are shown in **S1 Data.**
517
518 **ACKNOWLEDGEMENTS**
519 We thank Valerie Borde for the strain with Zip3-FLAG construct and Scott Keeney and Hajime
520 Murakami for the R script for scaling ChIP-Seq data. We thank Eric Alani and Michael Lichten
521 and Valerie Borde for discussions on the manuscript.
522
523
524

525 **REFERENCES**

526 1. Neale MJ, Keeney S. Clarifying the mechanics of DNA strand exchange in meiotic
527 recombination. Nature. 2006;442(7099):153-8. doi: 10.1038/nature04885. PubMed PMID:
528 16838012.
529 2. Keeney S, Giroux CN, Kleckner N. Meiosis-specific DNA double-strand breaks are
530 catalyzed by Spo11, a member of a widely conserved protein family. Cell. 1997;88(3):375-84.
531 PubMed PMID: 9039264.
532 3. Bergerat A, de Massy B, Gadelle D, Varoutas PC, Nicolas A, Forterre P. An atypical
533 topoisomerase II from Archaea with implications for meiotic recombination. Nature.
534 1997;386(6623):414-7. doi: 10.1038/386414a0. PubMed PMID: 9121560.
535 4. Petronczki M, Siomos MF, Nasmyth K. Un menage a quatre: the molecular biology of
536 chromosome segregation in meiosis. Cell. 2003;112(4):423-40. PubMed PMID: 12600308.
537 5. Allers T, Lichten M. Differential timing and control of noncrossover and crossover
538 recombination during meiosis. Cell. 2001;106(1):47-57. PubMed PMID: 11461701.
539 6. Hunter N, Kleckner N. The single-end invasion: an asymmetric intermediate at the
540 double-strand break to double-holliday junction transition of meiotic recombination. Cell.
541 2001;106(1):59-70. PubMed PMID: 11461702.
542 7. Page SL, Hawley RS. Chromosome choreography: the meiotic ballet. Science.
543 2003;301(5634):785-9. doi: 10.1126/science.1086605. PubMed PMID: 12907787.
544 8. Petes TD. Meiotic recombination hot spots and cold spots. Nature Reviews Genetics.
545 2001;2(5):360-9. doi: 10.1038/35072078. PubMed PMID: 11331902.
546 9. Buhler C, Borde V, Lichten M. Mapping meiotic single-strand DNA reveals a new
547 landscape of DNA double-strand breaks in Saccharomyces cerevisiae. PLoS Biology.

548 2007;5(12):e324. doi: 10.1371/journal.pbio.0050324. PubMed PMID: 18076285; PubMed
549 Central PMCID: PMC2121111.
550 10. Smith AV, Roeder GS. The yeast Red1 protein localizes to the cores of meiotic
551 chromosomes. The Journal of Cell Biology. 1997;136(5):957-67. PubMed PMID: 9060462;
552 PubMed Central PMCID: PMC2132480.
553 11. Zickler D, Kleckner N. A few of our favorite things: Pairing, the bouquet, crossover
554 interference and evolution of meiosis. Seminars in Cell & Developmental Biology. 2016;54:135-
555 48. doi: 10.1016/j.semcdb.2016.02.024. PubMed PMID: 26927691; PubMed Central PMCID:
556 PMC4867269.
557 12. Zickler D, Kleckner N. Meiotic chromosomes: integrating structure and function. Annual
558 Review of Genetics. 1999;33:603-754. doi: 10.1146/annurev.genet.33.1.603. PubMed PMID:
559 10690419.
560 13. Hollingsworth NM, Goetsch L, Byers B. The HOP1 gene encodes a meiosis-specific
561 component of yeast chromosomes. Cell. 1990;61(1):73-84. PubMed PMID: 2107981.
562 14. Klein F, Mahr P, Galova M, Buonomo SB, Michaelis C, Nairz K, et al. A central role for
563 cohesins in sister chromatid cohesion, formation of axial elements, and recombination during
564 yeast meiosis. Cell. 1999;98(1):91-103. doi: 10.1016/S0092-8674(00)80609-1. PubMed PMID:
565 10412984.
566 15. Sun X, Huang L, Markowitz TE, Blitzblau HG, Chen D, Klein F, et al. Transcription
567 dynamically patterns the meiotic chromosome-axis interface. eLife. 2015;4. doi:
568 10.7554/eLife.07424. PubMed PMID: 26258962; PubMed Central PMCID: PMC4530585.

569 16. Blat Y, Protacio RU, Hunter N, Kleckner N. Physical and functional interactions among
570 basic chromosome organizational features govern early steps of meiotic chiasma formation. Cell.
571 2002;111(6):791-802. PubMed PMID: 12526806.
572 17. Borde V, de Massy B. Programmed induction of DNA double strand breaks during
573 meiosis: setting up communication between DNA and the chromosome structure. Current
574 opinion in Genetics & Development. 2013;23(2):147-55. doi: 10.1016/j.gde.2012.12.002.
575 PubMed PMID: 23313097.
576 18. Pan J, Sasaki M, Kniewel R, Murakami H, Blitzblau HG, Tischfield SE, et al. A
577 hierarchical combination of factors shapes the genome-wide topography of yeast meiotic
578 recombination initiation. Cell. 2011;144(5):719-31. doi: 10.1016/j.cell.2011.02.009. PubMed
579 PMID: 21376234; PubMed Central PMCID: PMCPMC3063416.
580 19. Panizza S, Mendoza MA, Berlinger M, Huang L, Nicolas A, Shirahige K, et al. Spo11-
581 accessory proteins link double-strand break sites to the chromosome axis in early meiotic
582 recombination. Cell. 2011;146(3):372-83. doi: 10.1016/j.cell.2011.07.003. PubMed PMID:
583 21816273.
584 20. Kleckner N. Chiasma formation: chromatin/axis interplay and the role(s) of the
585 synaptonemal complex. Chromosoma. 2006;115(3):175-94. doi: 10.1007/s00412-006-0055-7.
586 PubMed PMID: 16555016.
587 21. Acquaviva L, Szekvolgyi L, Dichtl B, Dichtl BS, de La Roche Saint Andre C, Nicolas A,
588 et al. The COMPASS subunit Spp1 links histone methylation to initiation of meiotic
589 recombination. Science. 2013;339(6116):215-8. doi: 10.1126/science.1225739. PubMed PMID:
590 23160953.

591 22. Sommermeyer V, Beneut C, Chaplais E, Serrentino ME, Borde V. Spp1, a member of the
592 Set1 Complex, promotes meiotic DSB formation in promoters by tethering histone H3K4
593 methylation sites to chromosome axes. Molecular Cell. 2013;49(1):43-54. doi:
594 10.1016/j.molcel.2012.11.008. PubMed PMID: 23246437.
595 23. Medhi D, Goldman AS, Lichten M. Local chromosome context is a major determinant of
596 crossover pathway biochemistry during budding yeast meiosis. eLife. 2016;5. doi:
597 10.7554/eLife.19669. PubMed PMID: 27855779; PubMed Central PMCID: PMC5222560.
598 24. Borner GV, Kleckner N, Hunter N. Crossover/noncrossover differentiation,
599 synaptonemal complex formation, and regulatory surveillance at the leptotene/zygotene
600 transition of meiosis. Cell. 2004;117(1):29-45. PubMed PMID: 15066280.
601 25. Shinohara M, Oh SD, Hunter N, Shinohara A. Crossover assurance and crossover
602 interference are distinctly regulated by the ZMM proteins during yeast meiosis. Nature Genetics.
603 2008;40(3):299-309. doi: 10.1038/ng.83. PubMed PMID: 18297071.
604 26. Lynn A, Soucek R, Borner GV. ZMM proteins during meiosis: crossover artists at work.
605 Chromosome Research. 2007;15(5):591-605. doi: 10.1007/s10577-007-1150-1. PubMed PMID:
606 17674148.
607 27. Manhart CM, Ni X, White MA, Ortega J, Surtees JA, Alani E. The mismatch repair and
608 meiotic recombination endonuclease Mlh1-Mlh3 is activated by polymer formation and can
609 cleave DNA substrates in trans. PLoS Biology. 2017;15(4):e2001164. doi:
610 10.1371/journal.pbio.2001164. PubMed PMID: 28453523; PubMed Central PMCID:
611 PMC5409509.
612 28. Zakharyevich K, Ma Y, Tang S, Hwang PY, Boiteux S, Hunter N. Temporally and
613 biochemically distinct activities of Exo1 during meiosis: double-strand break resection and

614 resolution of double Holliday junctions. Molecular Cell. 2010;40(6):1001-15. doi:
615 10.1016/j.molcel.2010.11.032. PubMed PMID: 21172664; PubMed Central PMCID:
616 PMC3061447.
617 29. de los Santos T, Hunter N, Lee C, Larkin B, Loidl J, Hollingsworth NM. The
618 Mus81/Mms4 endonuclease acts independently of double-Holliday junction resolution to
619 promote a distinct subset of crossovers during meiosis in budding yeast. Genetics.
620 2003;164(1):81-94. PubMed PMID: 12750322; PubMed Central PMCID: PMCPMC1462551.
621 30. Argueso JL, Wanat J, Gemici Z, Alani E. Competing crossover pathways act during
622 meiosis in Saccharomyces cerevisiae. Genetics. 2004;168(4):1805-16. doi:
623 10.1534/genetics.104.032912. PubMed PMID: 15611158; PubMed Central PMCID:
624 PMCPMC1448724.
625 31. Ross-Macdonald P, Roeder GS. Mutation of a meiosis-specific MutS homolog decreases
626 crossing over but not mismatch correction. Cell. 1994;79(6):1069-80. PubMed PMID: 8001134.
627 32. Pochart P, Woltering D, Hollingsworth NM. Conserved properties between functionally
628 distinct MutS homologs in yeast. J Biol Chem. 1997;272(48):30345-9. doi: DOI
629 10.1074/jbc.272.48.30345. PubMed PMID: WOS:A1997YH61300055.
630 33. Hollingsworth NM, Ponte L, Halsey C. MSH5, a novel MutS homolog, facilitates meiotic
631 reciprocal recombination between homologs in Saccharomyces cerevisiae but not mismatch
632 repair. Genes & Development. 1995;9(14):1728-39. PubMed PMID: 7622037.
633 34. Snowden T, Acharya S, Butz C, Berardini M, Fishel R. hMSH4-hMSH5 recognizes
634 Holliday Junctions and forms a meiosis-specific sliding clamp that embraces homologous
635 chromosomes. Molecular Cell. 2004;15(3):437-51. doi: 10.1016/j.molcel.2004.06.040. PubMed
636 PMID: 15304223.

637 35. Lahiri S, Li Y, Hingorani MM, Mukerji I. MutSgamma-Induced DNA conformational
638 changes provide insights into its role in meiotic recombination. Biophysical Journal.
639 2018;115(11):2087-101. Epub 2018/11/24. doi: 10.1016/j.bpj.2018.10.029. PubMed PMID:
640 30467025; PubMed Central PMCID: PMCPMC6289823.
641 36. He W, Rao H, Tang S, Bhagwat N, Kulkarni DS, Ma Y, et al. Regulated proteolysis of
642 MutSgamma controls meiotic crossing over. Molecular Cell. 2020;78(1):168-83 e5. Epub
643 2020/03/05. doi: 10.1016/j.molcel.2020.02.001. PubMed PMID: 32130890.
644 37. Nishant KT, Plys AJ, Alani E. A mutation in the putative MLH3 endonuclease domain
645 confers a defect in both mismatch repair and meiosis in Saccharomyces cerevisiae. Genetics.
646 2008;179(2):747-55. doi: 10.1534/genetics.108.086645. PubMed PMID: 18505871; PubMed
647 Central PMCID: PMCPMC2429871.
648 38. Zakharyevich K, Tang S, Ma Y, Hunter N. Delineation of joint molecule resolution
649 pathways in meiosis identifies a crossover-specific resolvase. Cell. 2012;149(2):334-47. doi:
650 10.1016/j.cell.2012.03.023. PubMed PMID: 22500800; PubMed Central PMCID:
651 PMCPMC3377385.
652 39. Kolas NK, Svetlanov A, Lenzi ML, Macaluso FP, Lipkin SM, Liskay RM, et al.
653 Localization of MMR proteins on meiotic chromosomes in mice indicates distinct functions
654 during prophase I. The Journal of Cell Biology. 2005;171(3):447-58. doi:
655 10.1083/jcb.200506170. PubMed PMID: 16260499; PubMed Central PMCID: PMC2171243.
656 40. Cannavo E, Sanchez A, Anand R, Ranjha L, Hugener J, Adam C, et al. Regulation of the
657 MLH1-MLH3 endonuclease in meiosis. 2020:2020.02.12.946293. doi:
658 10.1101/2020.02.12.946293 %J bioRxiv.

659 41. Kulkarni DS, Owens S, Honda M, Ito M, Yang Y, Corrigan MW, et al. PCNA activates
660 the MutLγ endonuclease to promote meiotic crossing over. 2020:2020.02.12.946020. doi:
661 10.1101/2020.02.12.946020 %J bioRxiv.
662 42. Kneitz B, Cohen PE, Avdievich E, Zhu L, Kane MF, Hou H, Jr., et al. MutS homolog 4
663 localization to meiotic chromosomes is required for chromosome pairing during meiosis in male
664 and female mice. Genes & Development. 2000;14(9):1085-97. PubMed PMID: 10809667;
665 PubMed Central PMCID: PMC316572.
666 43. Edelmann W, Cohen PE, Kneitz B, Winand N, Lia M, Heyer J, et al. Mammalian MutS
667 homologue 5 is required for chromosome pairing in meiosis. Nature Genetics. 1999;21(1):123-7.
668 doi: 10.1038/5075. PubMed PMID: 9916805.
669 44. Cole F, Kauppi L, Lange J, Roig I, Wang R, Keeney S, et al. Homeostatic control of
670 recombination is implemented progressively in mouse meiosis. Nature Cell Biology.
671 2012;14(4):424-30. doi: 10.1038/ncb2451. PubMed PMID: 22388890; PubMed Central PMCID:
672 PMC3319518.
673 45. Svetlanov A, Cohen PE. Mismatch repair proteins, meiosis, and mice: understanding the
674 complexities of mammalian meiosis. Experimental Cell Research. 2004;296(1):71-9. doi:
675 10.1016/j.yexcr.2004.03.020. PubMed PMID: 15120996.
676 46. Santucci-Darmanin S, Walpita D, Lespinasse F, Desnuelle C, Ashley T, Paquis-
677 Flucklinger V. MSH4 acts in conjunction with MLH1 during mammalian meiosis. FASEB
678 Journal. 2000;14(11):1539-47. PubMed PMID: 10928988.
679 47. De Muyt A, Pyatnitskaya A, Andreani J, Ranjha L, Ramus C, Laureau R, et al. A meiotic
680 XPF-ERCC1-like complex recognizes joint molecule recombination intermediates to promote
681 crossover formation. Genes & Development. 2018;32(3-4):283-96. doi:

682 10.1101/gad.308510.117. PubMed PMID: 29440262; PubMed Central PMCID:
683 PMCPMC5859969.
684 48. Serrentino ME, Chaplais E, Sommermeyer V, Borde V. Differential association of the
685 conserved SUMO ligase Zip3 with meiotic double-strand break sites reveals regional variations
686 in the outcome of meiotic recombination. PLoS Genetics. 2013;9(4):e1003416. doi:
687 10.1371/journal.pgen.1003416. PubMed PMID: 23593021; PubMed Central PMCID:
688 PMCPMC3616913.
689 49. Shinohara M, Hayashihara K, Grubb JT, Bishop DK, Shinohara A. DNA damage
690 response clamp 9-1-1 promotes assembly of ZMM proteins for formation of crossovers and
691 synaptonemal complex. Journal of Cell Science. 2015;128(8):1494-506. doi:
692 10.1242/jcs.161554. PubMed PMID: 25736290; PubMed Central PMCID: PMCPMC4518444.
693 50. Nishant KT, Chen C, Shinohara M, Shinohara A, Alani E. Genetic analysis of baker's
694 yeast Msh4-Msh5 reveals a threshold crossover level for meiotic viability. PLoS Genetics.
695 2010;6(8). doi: 10.1371/journal.pgen.1001083. PubMed PMID: 20865162; PubMed Central
696 PMCID: PMCPMC2928781.
697 51. Mimitou EP, Yamada S, Keeney S. A global view of meiotic double-strand break end
698 resection. Science. 2017;355(6320):40-5. doi: 10.1126/science.aak9704. PubMed PMID:
699 28059759; PubMed Central PMCID: PMC5234563.
700 52. Bishop DK, Park D, Xu L, Kleckner N. DMC1: a meiosis-specific yeast homolog of E.
701 coli recA required for recombination, synaptonemal complex formation, and cell cycle
702 progression. Cell. 1992;69(3):439-56. PubMed PMID: 1581960.
703 53. Lao JP, Cloud V, Huang CC, Grubb J, Thacker D, Lee CY, et al. Meiotic crossover
704 control by concerted action of Rad51-Dmc1 in homolog template bias and robust homeostatic

705 regulation. PLoS Genetics. 2013;9(12):e1003978. doi: 10.1371/journal.pgen.1003978. PubMed
706 PMID: 24367271; PubMed Central PMCID: PMCPMC3868528.
707 54. Cloud V, Chan YL, Grubb J, Budke B, Bishop DK. Rad51 is an accessory factor for
708 Dmc1-mediated joint molecule formation during meiosis. Science. 2012;337(6099):1222-5. doi:
709 10.1126/science.1219379. PubMed PMID: 22955832; PubMed Central PMCID:
710 PMCPMC4056682.
711 55. Lao JP, Oh SD, Shinohara M, Shinohara A, Hunter N. Rad52 promotes postinvasion
712 steps of meiotic double-strand-break repair. Molecular Cell. 2008;29(4):517-24. doi:
713 10.1016/j.molcel.2007.12.014. PubMed PMID: 18313389; PubMed Central PMCID:
714 PMC2351957.
715 56. Bishop DK. RecA homologs Dmc1 and Rad51 interact to form multiple nuclear
716 complexes prior to meiotic chromosome synapsis. Cell. 1994;79(6):1081-92. PubMed PMID:
717 7528104.
718 57. Murakami H, Lam I, Huang PC, Song J, van Overbeek M, Keeney S. Multilayered
719 mechanisms ensure that short chromosomes recombine in meiosis. Nature. 2020;582(7810):124-
720 8. Epub 2020/06/05. doi: 10.1038/s41586-020-2248-2. PubMed PMID: 32494071; PubMed
721 Central PMCID: PMCPMC7298877.
722 58. Chakraborty P, Pankajam AV, Lin G, Dutta A, Krishnaprasad GN, Tekkedil MM, et al.
723 Modulating crossover frequency and interference for obligate crossovers in Saccharomyces
724 cerevisiae meiosis. G3 (Bethesda). 2017;7(5):1511-24. doi: 10.1534/g3.117.040071. PubMed
725 PMID: 28315832; PubMed Central PMCID: PMCPMC5427503.
726 59. Krishnaprasad GN, Anand MT, Lin G, Tekkedil MM, Steinmetz LM, Nishant KT.
727 Variation in crossover frequencies perturb crossover assurance without affecting meiotic

728 chromosome segregation in Saccharomyces cerevisiae. Genetics. 2015;199(2):399-412. Epub
729 2014/12/04. doi: 10.1534/genetics.114.172320. PubMed PMID: 25467183; PubMed Central
730 PMCID: PMCPMC4317650.
731 60. Prieler S, Penkner A, Borde V, Klein F. The control of Spo11's interaction with meiotic
732 recombination hotspots. Genes & Development. 2005;19(2):255-69. doi: 10.1101/gad.321105.
733 PubMed PMID: 15655113; PubMed Central PMCID: PMC545890.
734 61. Schwacha A, Kleckner N. Interhomolog bias during meiotic recombination: meiotic
735 functions promote a highly differentiated interhomolog-only pathway. Cell. 1997;90(6):1123-35.
736 PubMed PMID: 9323140.
737 62. Carballo JA, Johnson AL, Sedgwick SG, Cha RS. Phosphorylation of the axial element
738 protein Hop1 by Mec1/Tel1 ensures meiotic interhomolog recombination. Cell.
739 2008;132(5):758-70. doi: 10.1016/j.cell.2008.01.035. PubMed PMID: 18329363.
740 63. Kim KP, Weiner BM, Zhang L, Jordan A, Dekker J, Kleckner N. Sister cohesion and
741 structural axis components mediate homolog bias of meiotic recombination. Cell.
742 2010;143(6):924-37. doi: 10.1016/j.cell.2010.11.015. PubMed PMID: 21145459; PubMed
743 Central PMCID: PMC3033573.
744 64. Evans E, Sugawara N, Haber JE, Alani E. The Saccharomyces cerevisiae Msh2 mismatch
745 repair protein localizes to recombination intermediates in vivo. Molecular Cell. 2000;5(5):789-
746 99. PubMed PMID: 10882115.
747 65. Agarwal S, Roeder GS. Zip3 provides a link between recombination enzymes and
748 synaptonemal complex proteins. Cell. 2000;102(2):245-55. PubMed PMID: 10943844.

749 66. Pyatnitskaya A, Borde V, De Muyt A. Crossing and zipping: molecular duties of the
750 ZMM proteins in meiosis. Chromosoma. 2019;128(3):181-98. Epub 2019/06/27. doi:
751 10.1007/s00412-019-00714-8. PubMed PMID: 31236671.
752 67. Tsubouchi T, Macqueen AJ, Roeder GS. Initiation of meiotic chromosome synapsis at
753 centromeres in budding yeast. Genes & Development. 2008;22(22):3217-26. Epub 2008/12/06.
754 doi: 10.1101/gad.1709408. PubMed PMID: 19056898; PubMed Central PMCID:
755 PMCPMC2593611.
756 68. Hunter N, Borts RH. Mlh1 is unique among mismatch repair proteins in its ability to
757 promote crossing-over during meiosis. Genes & Development. 1997;11(12):1573-82. Epub
758 1997/06/15. doi: 10.1101/gad.11.12.1573. PubMed PMID: 9203583.
759 69. Kleckner N, Zickler D, Jones GH, Dekker J, Padmore R, Henle J, et al. A mechanical
760 basis for chromosome function. Proceedings of the National Academy of Sciences of the United
761 States of America. 2004;101(34):12592-7. doi: 10.1073/pnas.0402724101. PubMed PMID:
762 15299144; PubMed Central PMCID: PMC515102.
763 70. Zhang L, Wang S, Yin S, Hong S, Kim KP, Kleckner N. Topoisomerase II mediates
764 meiotic crossover interference. Nature. 2014;511(7511):551-6. doi: 10.1038/nature13442.
765 PubMed PMID: 25043020; PubMed Central PMCID: PMCPMC4128387.
766 71. Mortimer RK, Johnston JR. Genealogy of principal strains of the yeast genetic stock
767 center. Genetics. 1986;113(1):35-43. PubMed PMID: 3519363; PubMed Central PMCID:
768 PMC1202798.
769 72. Rose MD, F. Winston, and P. Hieter. Methods in yeast genetics. Cold Spring Harbor
770 Laboratory Press, Cold Spring Harbor, NY. 1990.

771 73. McCusker JH, Clemons KV, Stevens DA, Davis RW. Genetic characterization of
772 pathogenic Saccharomyces cerevisiae isolates. Genetics. 1994;136(4):1261-9. PubMed PMID:
773 8013903; PubMed Central PMCID: PMC1205906.
774 74. Gietz RD, Schiestl RH, Willems AR, Woods RA. Studies on the transformation of intact
775 yeast cells by the LiAc/SS-DNA/PEG procedure. Yeast. 1995;11(4):355-60. doi:
776 10.1002/yea.320110408. PubMed PMID: 7785336.
777 75. Goldstein AL, McCusker JH. Three new dominant drug resistance cassettes for gene
778 disruption in Saccharomyces cerevisiae. Yeast. 1999;15(14):1541-53. doi: 10.1002/(SICI)1097-
779 0061(199910)15:14<1541::AID-YEA476>3.0.CO;2-K. PubMed PMID: 10514571.
780 76. Thacker D, Mohibullah N, Zhu X, Keeney S. Homologue engagement controls meiotic
781 DNA break number and distribution. Nature. 2014;510(7504):241-6. doi: 10.1038/nature13120.
782 PubMed PMID: 24717437; PubMed Central PMCID: PMC4057310.
783 77. Mendoza MA, Panizza S, Klein F. Analysis of protein-DNA interactions during meiosis
784 by quantitative chromatin immunoprecipitation (qChIP). Methods in Molecular Biology.
785 2009;557:267-83. doi: 10.1007/978-1-59745-527-5_17. PubMed PMID: 19799188.
786 78. Liang K, Keles S. Normalization of ChIP-seq data with control. BMC Bioinformatics.
787 2012;13:199. doi: 10.1186/1471-2105-13-199. PubMed PMID: 22883957; PubMed Central
788 PMCID: PMC3475056.
789 79. Zhang Y, Liu T, Meyer CA, Eeckhoute J, Johnson DS, Bernstein BE, et al. Model-based
790 analysis of ChIP-Seq (MACS). Genome Biology. 2008;9(9):R137. doi: 10.1186/gb-2008-9-9-
791 r137. PubMed PMID: 18798982; PubMed Central PMCID: PMC2592715.
792 80. Murakami H, Keeney S. Temporospatial coordination of meiotic DNA replication and
793 recombination via DDK recruitment to replisomes. Cell. 2014;158(4):861-73. Epub 2014/08/16.

794 doi: 10.1016/j.cell.2014.06.028. PubMed PMID: 25126790; PubMed Central PMCID:
795 PMCPMC4141489.

796

797 **FIGURE LEGENDS**

798 **Fig 1. Msh5 expression and DNA binding in wild-type meiosis.** (**A)** Western blot analysis of
799 Msh5 expression pattern in synchronized wild-type meiosis. **(B)** ChIP using Msh5 antibody in
800 wild type and *msh5Δ* strains. Lanes 1 to 3 indicate lysate, lysate after overnight incubation with
801 Msh5 antibody and beads, and the eluate fractions in wild type. Lanes 4 to 6 indicate lysate,
802 lysate after overnight incubation with Msh5 antibody and beads and the eluate fractions in
803 *msh5Δ.* **C)** Msh5 enrichment at DSB hotspots (*BUD23*, *ECM3,* and *CCT6*), centromere regions
804 (*CEN I, CEN III*) and axis regions (*AXIS I*, *AXIS II*, *AXIS III*) relative to DSB coldspot
805 (*YCR093W*), measured using ChIP-qPCR. The samples are normalized using input. The error
806 bars represent the standard deviation.

807

808 **Fig 2. Msh5 binds at DSB hotspots, chromosome axis, and centromere positions. A)**
809 Density of scaled Msh5 ChIP-Seq reads at Msh5 peak locations (5h) from 3h to 7h.
810 **B)** Representative image to show chromosomal localization of Msh5 in wild type on
811 chromosome III (t=3, 4, and 5h after induction of meiosis) using qPCR scaled ChIP-Seq data.
812 Zoomed in image of the centromeric region, axis region, one DSB hotspot (*BUD23*), and one
813 DSB coldspot (*YCR093W*) is also shown. Red1 and Spo11 data are taken from, Sun et al
814 2015[15] and Pan et al., 2011 [18]. The black circle indicates centromere. (**C)** Coverage
815 analysis of qPCR scaled Msh5 ChIP-Seq reads at Spo11 DSB hotspots (*** indicates $p < 0.001$,

816 outliers are removed). (**D)** Width of the Msh5 binding peaks (5h time point) at DSB hotspots
817 (not overlapping with Red1 sites) from all four Msh5 ChIP-Seq replicates.
818
819 **Fig 3. Msh5 association with chromosome axis and centromeres. A)** Coverage analysis of
820 qPCR scaled Msh5 ChIP-Seq reads at axis sites (Red1 peaks) (*** indicates $p < 0.001$, outliers
821 are removed). **B)** Coverage analysis of qPCR scaled Msh5 ChIP-Seq reads at centromere sites
822 (* indicates $p < 0.01$, outliers are removed).
823
824 **Fig 4**. **Msh5 binding is stimulated by meiotic DSB repair intermediates. A)** Representative
825 image of a spread meiotic nucleus from wild-type strain (t=5h) immunostained for Msh5 (red
826 foci). **B)** Representative image of a spread meiotic nucleus from *spo11*Δ*, dmc1*Δ*, rad52*Δ*,* and
827 *ndt80*Δ mutants (t=5h) immunostained for Msh5 (red foci). *spo11Δ* indicates the specificity of
828 the Msh5 antibody. (**C)** Kinetics of Msh5 foci and the percentage of meiotic nuclei positive for
829 Msh5 foci in synchronized meiosis in wild type and *dmc1Δ*, *rad52*Δ*, ndt80*Δ mutants.
830 Approximately 50 nuclei, each from two independent experiments, were assessed for each time
831 point (except *spo11Δ*, see Materials and Methods). The error bars represent the standard
832 deviation.
833
834 **Fig 5**. **Msh5 binding at DSB hotspots is dependent on DSB frequency. (A)** Log2 of Spo11
835 reads [18] at Msh5 enriched and depleted DSB hotspots. **B)** Spo11 peak density plotted as a
836 function of chromosome size [18]. **C)** Msh5 and Zip3 read density plotted as a function of
837 chromosome size. **D)** Msh5 and Zip3 read density as a function of chromosome size, excluding
838 the shortest chromosomes (I, III and VI).

839 **Fig 6. Msh5 association with chromosomes in *red1*Δ mutant.** Representative image of **A)**
840 Msh5 (t = 5h) and **B)** Rad51 (t = 3h) foci and kinetics of its accumulation in *red1Δ* mutant.
841 Approximately 50 nuclei, each from two independent experiments, were assessed for each time
842 point. The error bars represent the standard deviation. **(C)** Coverage analysis of qPCR scaled
843 Msh5 ChIP-Seq reads at Spo11 DSB hotspots, Red1 peaks, and centromere positions (***
844 indicates $p < 0.001$ and * indicates $p < 0.01$, outliers are removed).

845 **Fig 7. Model for the chromosomal localization of the Msh4-Msh5 complex during meiosis.**
846 During meiosis binding of the axis proteins (Red1/Hop1) define the chromosomal axis region
847 with intervening loop regions. The loops are recruited to the axis region for DSB formation.
848 Msh4-Msh5 associates with the DSB hotspots and axis after DSB formation at early stages (3h)
849 of meiosis. At later stages (4-5h), enhanced binding of Msh5 is observed at DSB hotspots
850 consistent with the generation of joint molecule structures that promote Msh5 binding. Also,
851 Msh5 is enriched at strong DSB hotspots. Msh5 binding to both loop and axis regions may
852 promote loop-axis interaction for crossover formation.
853
854 **S1 Fig. Genome-wide pairwise comparison of the log2 (fold change) of Msh5 reads for**
855 **wild-type replicates (a-d) (panels A-F).**
856
857 **S2 Fig. Msh5 binding sites from ChIP-Seq and ChIP-qPCR data. A)** NCIS normalized
858 Msh5 ChIP-Seq reads from all four replicates (not scaled with ChIP-qPCR) in wild type on
859 chromosome III (t=3, 4, and 5h after induction of meiosis). **B)** ChIP-qPCR analysis of Msh5
860 enrichment at representative DSB hotspots, axis regions, centromeres, and cold spot (*YCR093W*).
861

862 **S3 Fig. Linear regression model of Msh5 ChIP-Seq and ChIP-qPCR data. A)** Correlation
863 between Msh5 ChIP-qPCR and ChIP-Seq in wild-type strains at different time points (2 -7h) for
864 DSB hotspots (*BUD23*, *ECM3,* and *CCT6*), DSB coldspot (*YCR093W*), centromere regions
865 (*CEN I*, *CEN III*) and axis regions (*Axis I*, *Axis II*, *Axis III*). **B)** Correlation between Msh5 ChIP-
866 qPCR and ChIP-Seq in *red1*Δ (5h).
867
868 **S4 Fig. ChIP-qPCR scaled Msh5 ChIP-Seq coverage at centromere location on all**
869 **chromosomes for 3-6h time points.**
870
871 **S5 Fig. ChIP-qPCR analysis of Msh5 in meiotic mutants.** ChIP-qPCR analysis of Msh5
872 enrichment at DSB hotspots (*BUD23*, *ECM3,* and *CCT6*), DSB coldspot (*YCR093W*),
873 centromere regions (*CEN I, CEN III*) and axis regions (*Axis I*, *Axis II*, *Axis III*) in **A)** *msh5*Δ, **B)**
874 *msh4*Δ, **C)** *spo11*Δ and **D)** *red1*Δ mutants. The samples are normalized using input. The error
875 bars represent the standard deviation.
876
877 **S6 Fig. Zip3 ChIP-Seq analysis. A)** Western blot analysis of Zip3 expression in synchronized
878 wild-type meiosis. **B)** ChIP using anti-FLAG antibody in Zip3-FLAG and wild-type strains.
879 Lanes 1 to 6 indicate lysate fraction at 3, 4, and 5h time points. Lanes 7 to 12 indicate eluate
880 fractions at 3, 4, and 5h time points. **C)** Representative image of Zip3 binding on chromosome
881 III (t=3, 4, and 5h after induction of meiosis). Zoomed in image of the centromeric region, one
882 DSB hotspot (*YCR047C*), axis, and one DSB cold spot (*YCR093W*) is also shown.
883

884 **S7 Fig. Percentage of meiotic nuclei showing Msh5 aggregate like staining.** Approximately
885 50 nuclei, each from two independent experiments, were assessed for each time point (except
886 *spo11Δ*, see Materials and Methods).
887
888 **S1 Table. Msh5 peaks pooled from the four wild-type replicates (WT-a,b,c,d).** Peak start
889 and end positions are indicated.
890
891 **S2 Table. DSB hotspots that are enriched or depleted for Msh5.** DSB hotspot data (3600
892 hotspots) from Pan et al. 2011[18] were sorted based on overlap with Msh5 binding regions and
893 Spo11 oligo hits.
894
895 **S3 Table. List of strains used in this study.**
896
897 **S1 Data. Numerical data underlying all graphs in the manuscript.**

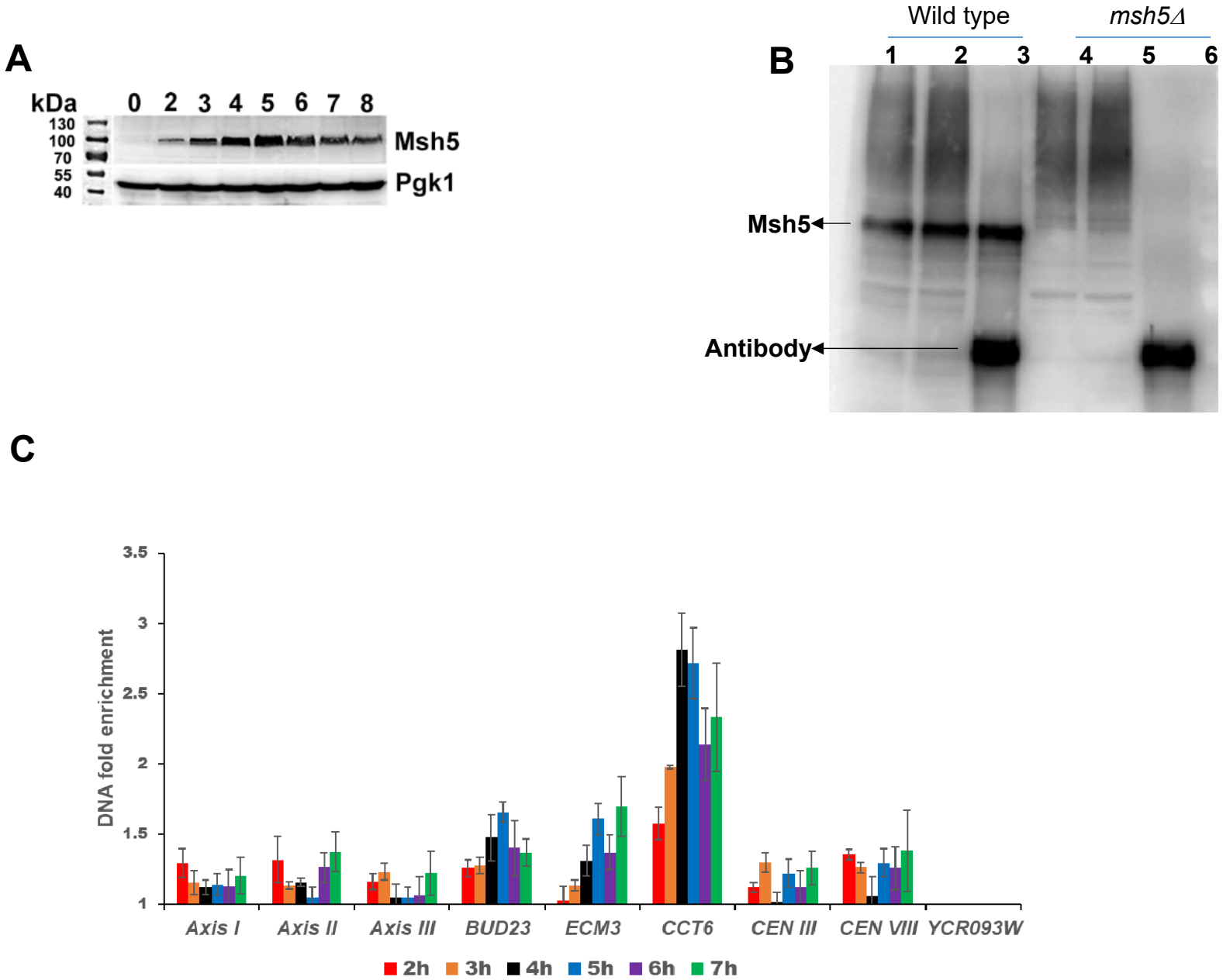
A
kDa
0 2 3 4 5 6 7 8
130
100
70
55
40
Msh5
Pgk1
B
Wild type
msh5Δ
1 2 3 4 5 6
Msh5
Antibody
C
DNA fold enrichment
3.5
3
2.5
2
1.5
1
Axis I
Axis II
Axis III
BUD23
ECM3
CCT6
CEN III
CEN VIII
YCR093W
2h
3h
4h
5h
6h
7h

Figure 1

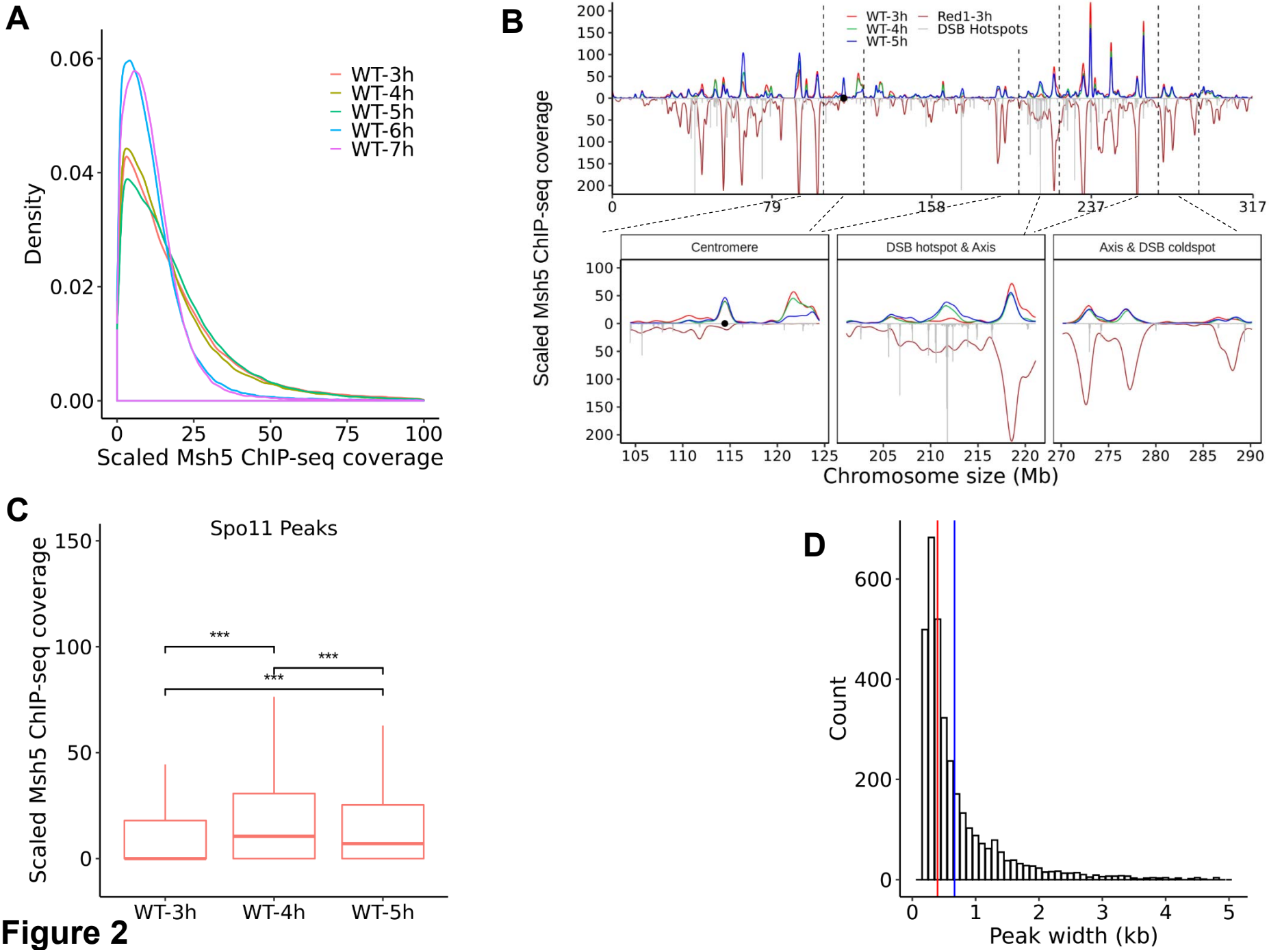
A
Density
0.06
0.04
0.02
0.00
WT-3h
WT-4h
WT-5h
WT-6h
WT-7h
0
25
50
75
100
Scaled Msh5 ChIP-seq coverage
B
Scaled Msh5 ChIP-seq coverage
WT-3h
WT-4h
WT-5h
Red1-3h
DSB Hotspots
0
79
158
237
317
Centromere
DSB hotspot & Axis
Axis & DSB coldspot
Chromosome size (Mb)
C
Spo11 Peaks
Scaled Msh5 ChIP-seq coverage
***
***
***
WT-3h
WT-4h
WT-5h
D
Count
Peak width (kb)

Figure 2

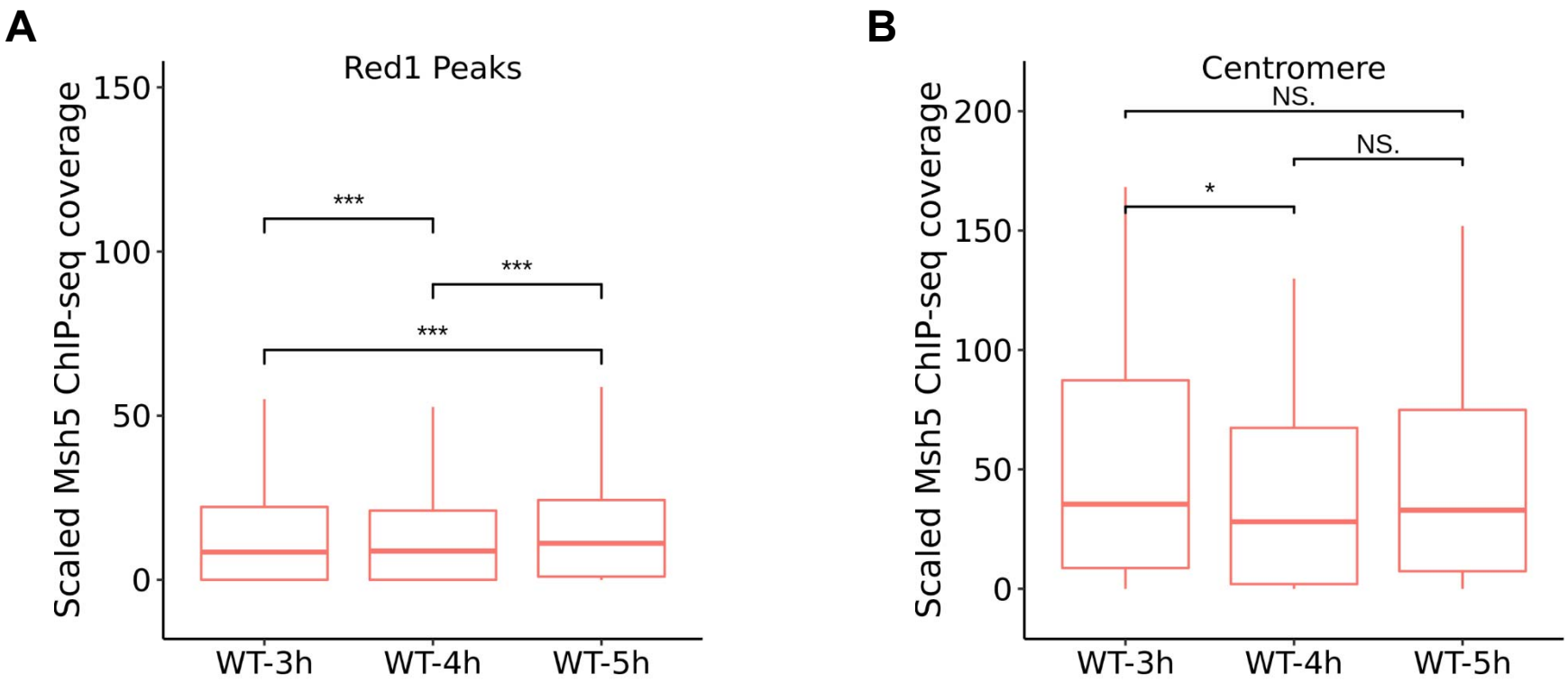
A
Red1 Peaks
Scaled Msh5 ChIP-seq coverage
150
100
50
0
***
***
***
WT-3h
WT-4h
WT-5h
B
Centromere
Scaled Msh5 ChIP-seq coverage
200
150
100
50
0
NS.
NS.
*
WT-3h
WT-4h
WT-5h

Figure 3

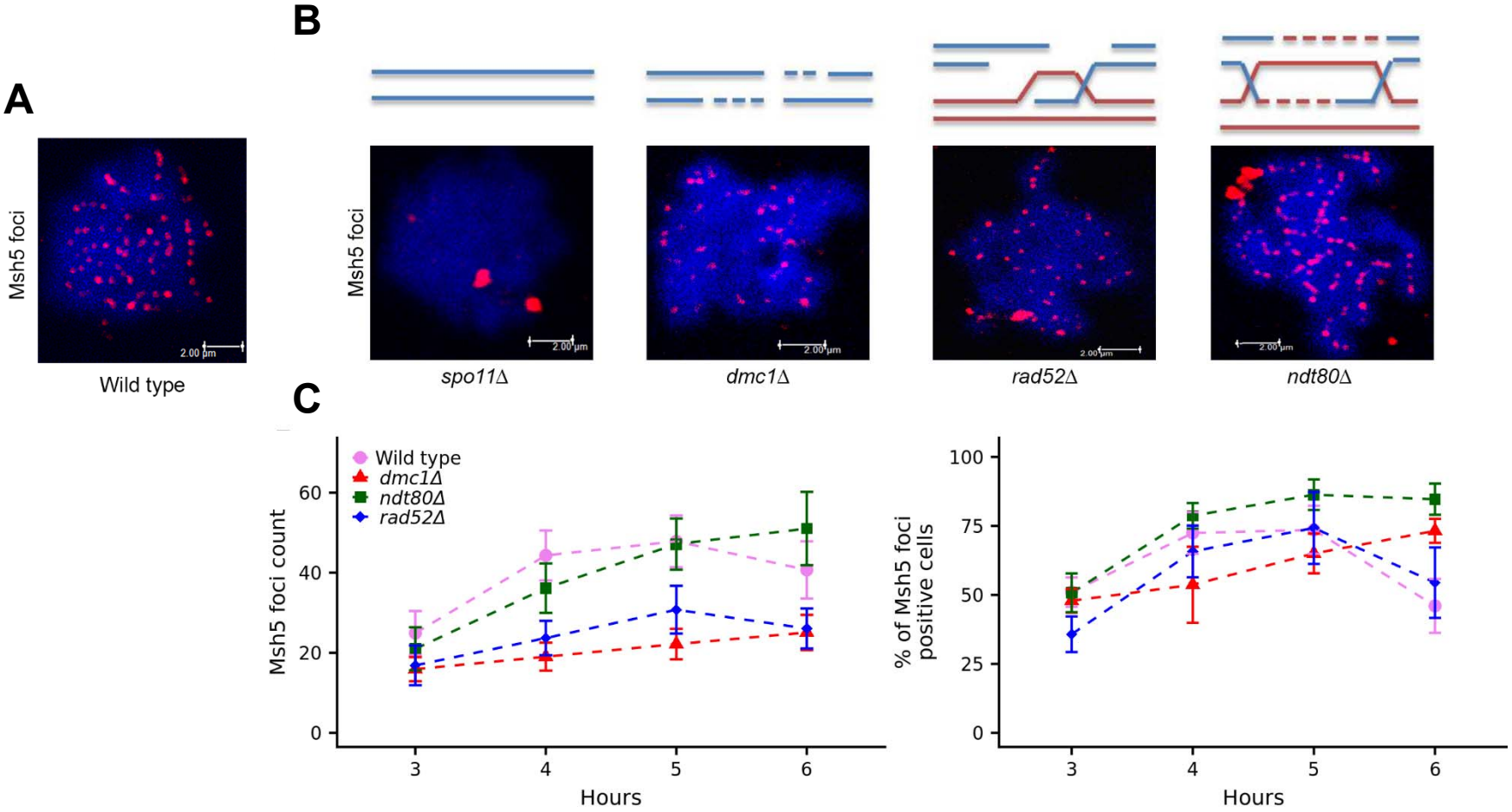
A
Msh5 foci
Wild type
B
Msh5 foci
spo11Δ
dmc1Δ
rad52Δ
ndt80Δ
C
Wild type
dmc1Δ
ndt80Δ
rad52Δ
Msh5 foci count
Hours
% of Msh5 foci positive cells
Hours

Figure 4

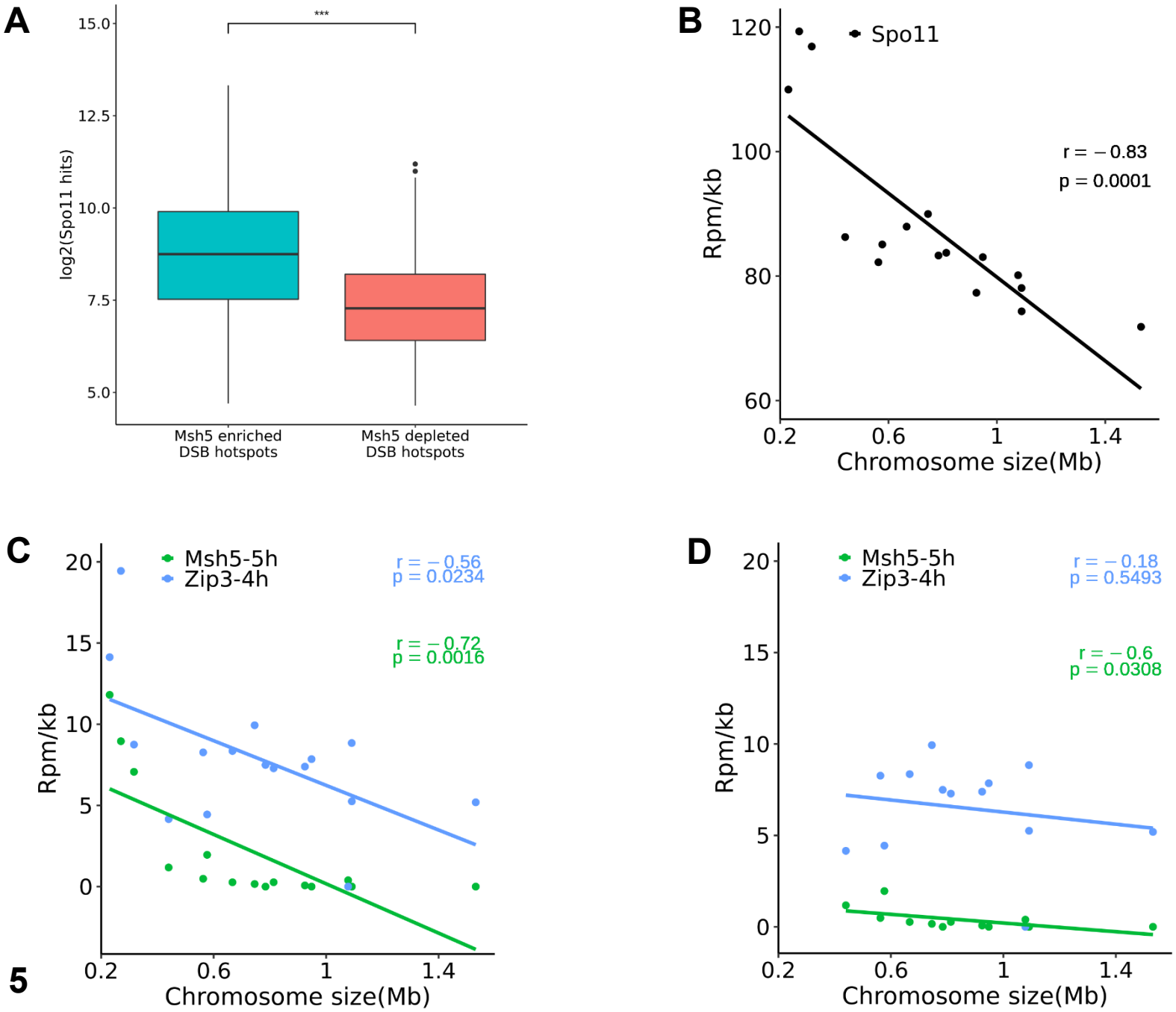
A
***
15.0
12.5
10.0
7.5
5.0
log2(Spo11 hits)
Msh5 enriched DSB hotspots
Msh5 depleted DSB hotspots
B
Spo11
r = −0.83
p = 0.0001
120
100
80
60
Rpm/kb
0.2
0.6
1
1.4
Chromosome size(Mb)
C
Msh5-5h
Zip3-4h
r = −0.56
p = 0.0234
r = −0.72
p = 0.0016
20
15
10
5
0
Rpm/kb
0.2
0.6
1
1.4
Chromosome size(Mb)
D
Msh5-5h
Zip3-4h
r = −0.18
p = 0.5493
r = −0.6
p = 0.0308
20
15
10
5
0
Rpm/kb
0.2
0.6
1
1.4
Chromosome size(Mb)

Figure 5

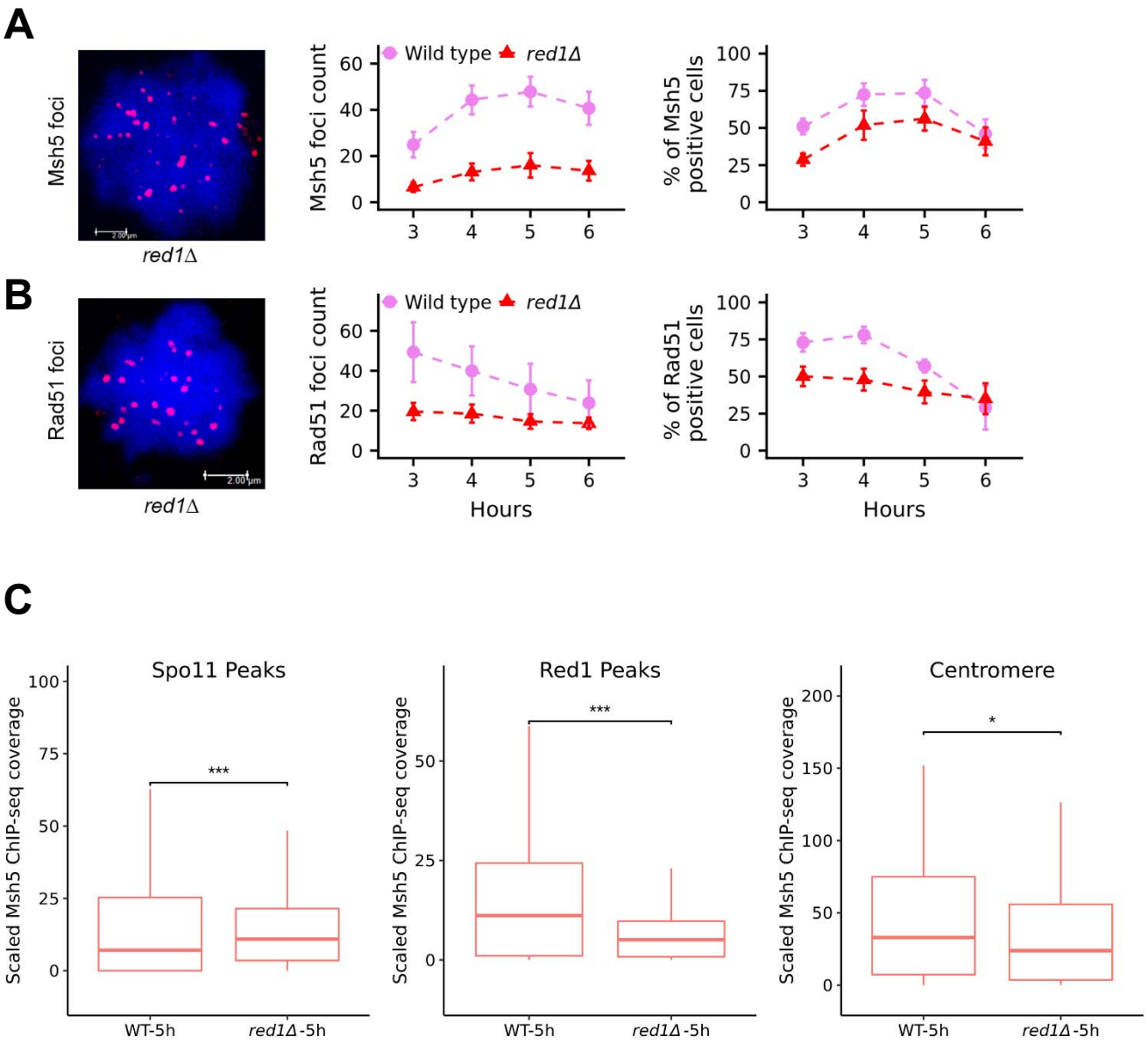
A
Msh5 foci
red1Δ
Wild type
red1Δ
Msh5 foci count
% of Msh5 positive cells
B
Rad51 foci
red1Δ
Rad51 foci count
% of Rad51 positive cells
Hours
C
Spo11 Peaks
Red1 Peaks
Centromere
Scaled Msh5 ChIP-seq coverage
WT-5h
red1Δ-5h

Figure 6

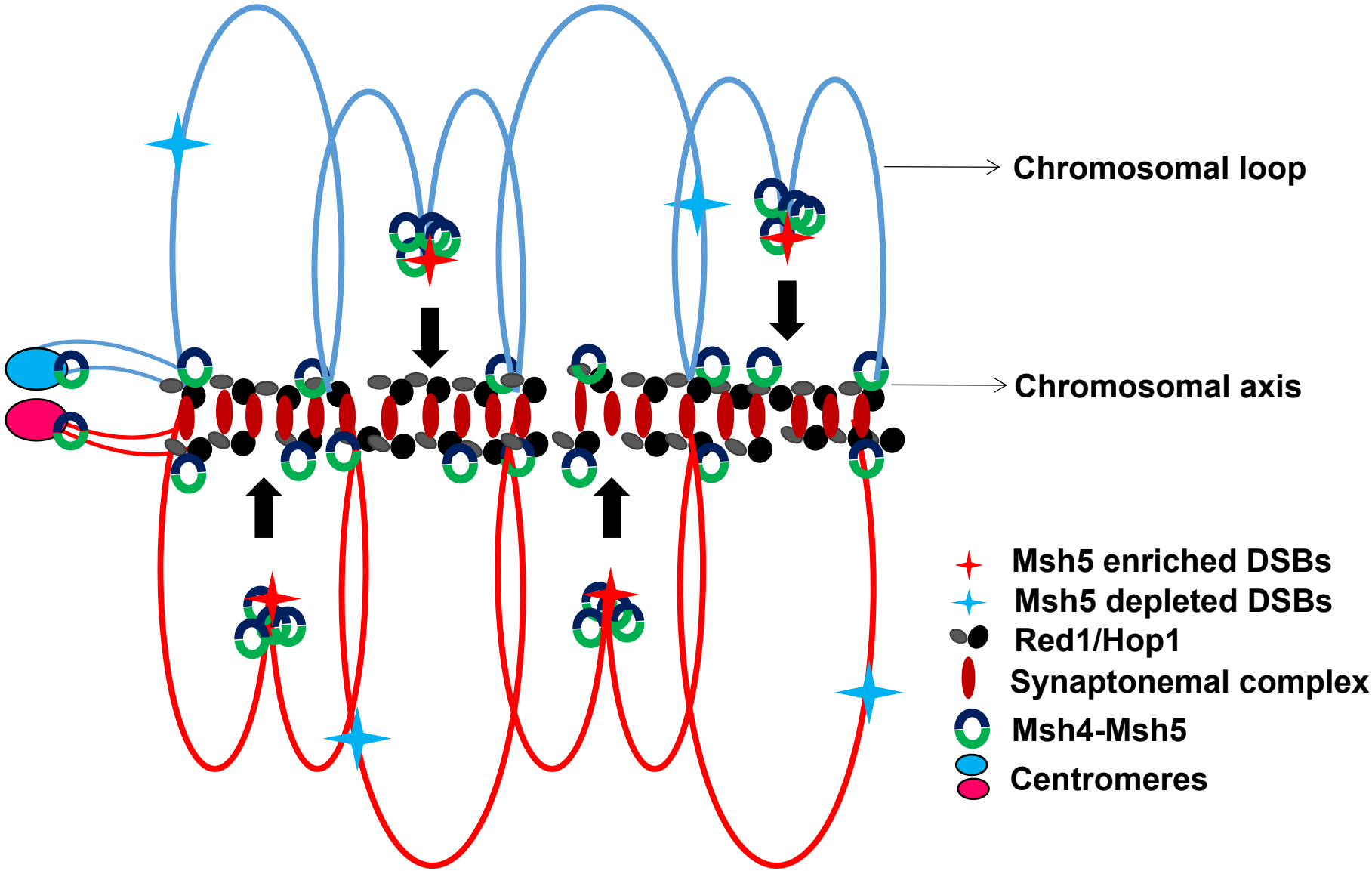
Chromosomal loop
Chromosomal axis
Msh5 enriched DSBs
Msh5 depleted DSBs
Red1/Hop1
Synaptonemal complex
Msh4-Msh5
Centromeres

Figure 7

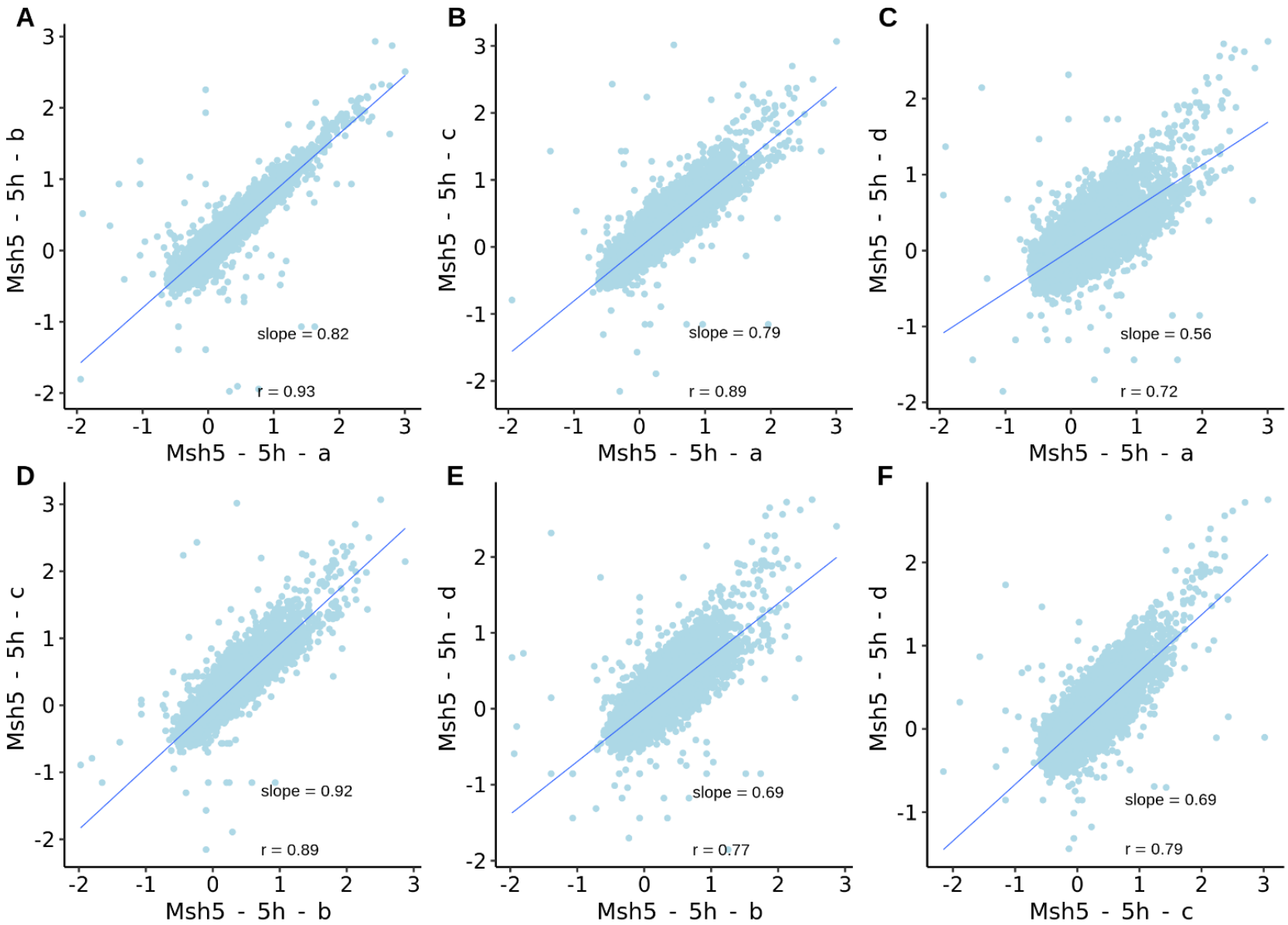
A
Msh5 - 5h - b
Msh5 - 5h - a
slope = 0.82
r = 0.93
B
Msh5 - 5h - c
Msh5 - 5h - a
slope = 0.79
r = 0.89
C
Msh5 - 5h - d
Msh5 - 5h - a
slope = 0.56
r = 0.72
D
Msh5 - 5h - c
Msh5 - 5h - b
slope = 0.92
r = 0.89
E
Msh5 - 5h - d
Msh5 - 5h - b
slope = 0.69
r = 0.77
F
Msh5 - 5h - d
Msh5 - 5h - c
slope = 0.69
r = 0.79

S1 Fig

A

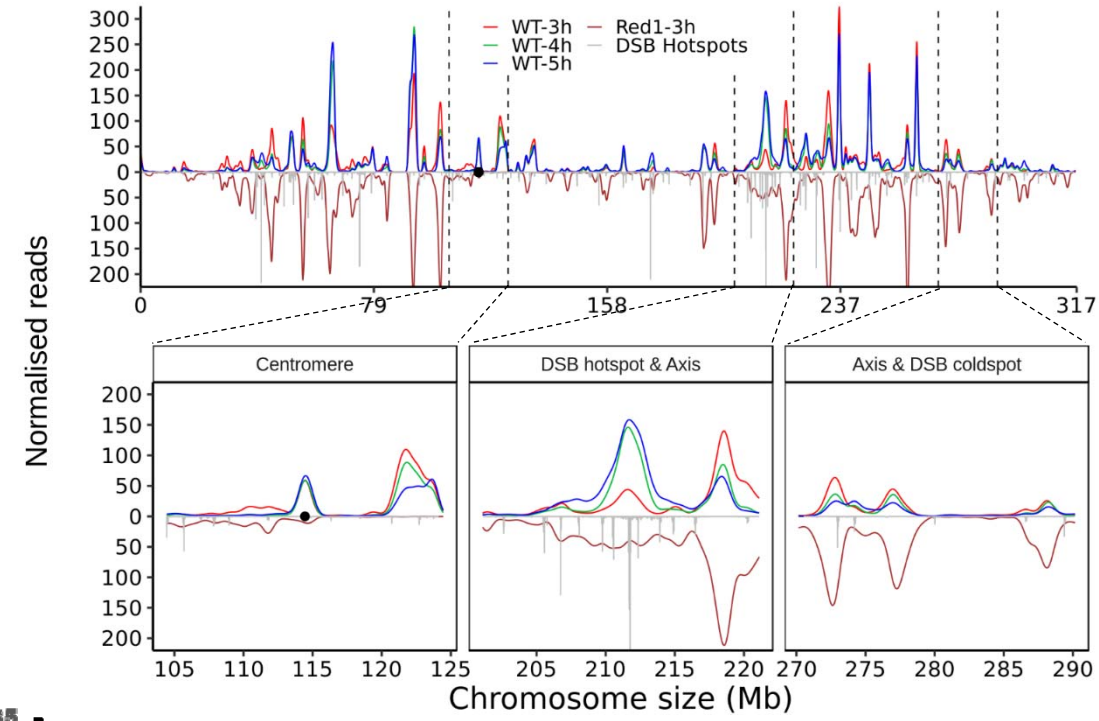
WT-3h
WT-4h
WT-5h
Red1-3h
DSB Hotspots
Normalised reads
Centromere
DSB hotspot & Axis
Axis & DSB coldspot
Chromosome size (Mb)

B

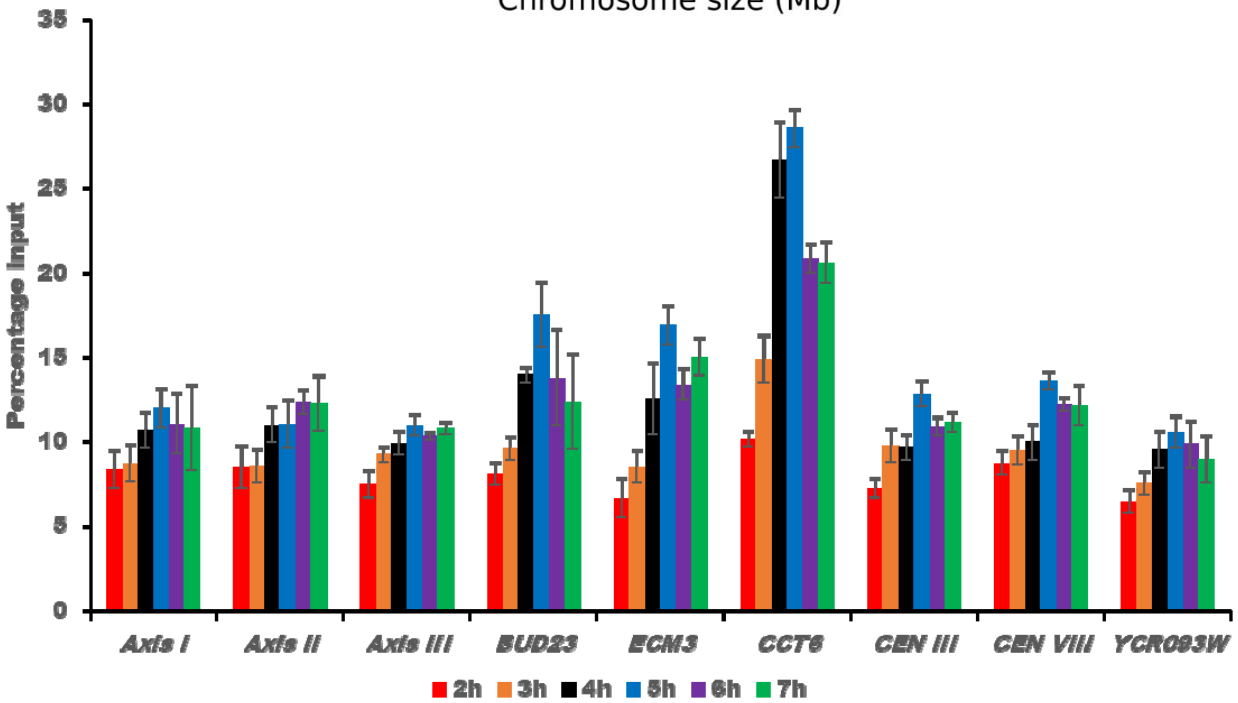
Percentage Input
Axis I
Axis II
Axis III
BUD23
ECM3
CCT6
CEN III
CEN VIII
YCR093W
2h
3h
4h
5h
6h
7h

S2 Fig

A **Wild type**

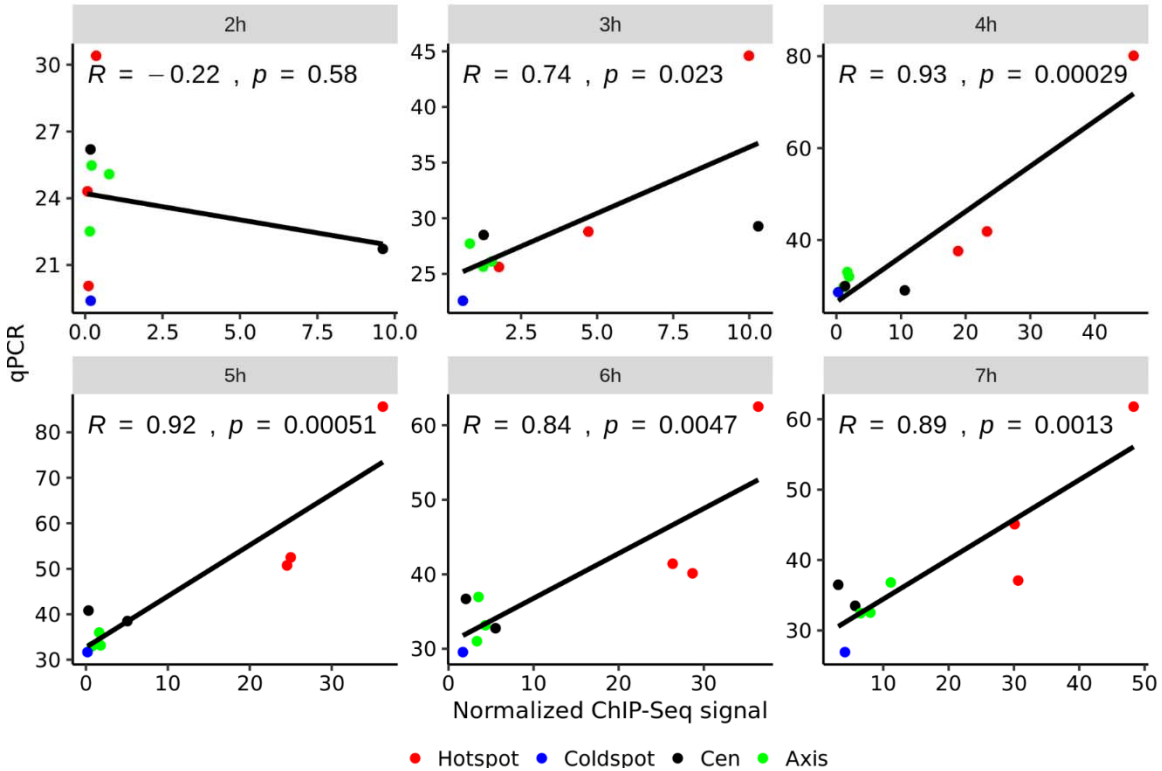

B ***red1*Δ**

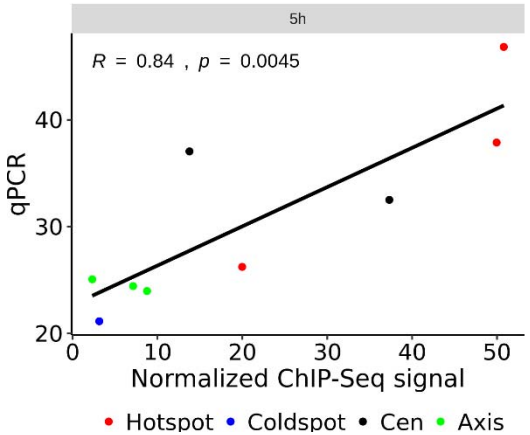

S3 Fig

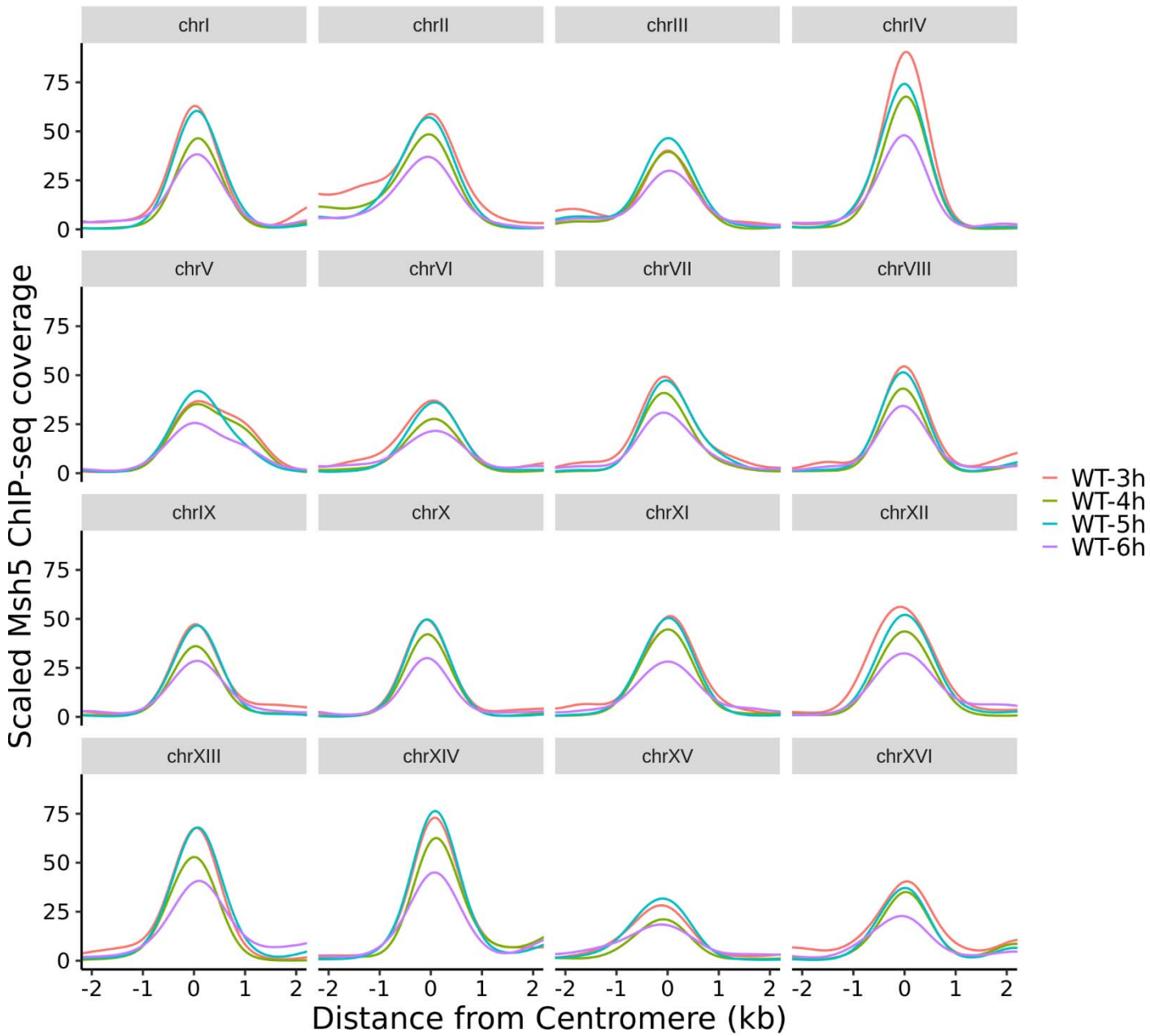
chrI
chrII
chrIII
chrIV
chrV
chrVI
chrVII
chrVIII
chrIX
chrX
chrXI
chrXII
chrXIII
chrXIV
chrXV
chrXVI
Scaled Msh5 ChIP-seq coverage
Distance from Centromere (kb)
WT-3h
WT-4h
WT-5h
WT-6h

S4 Fig

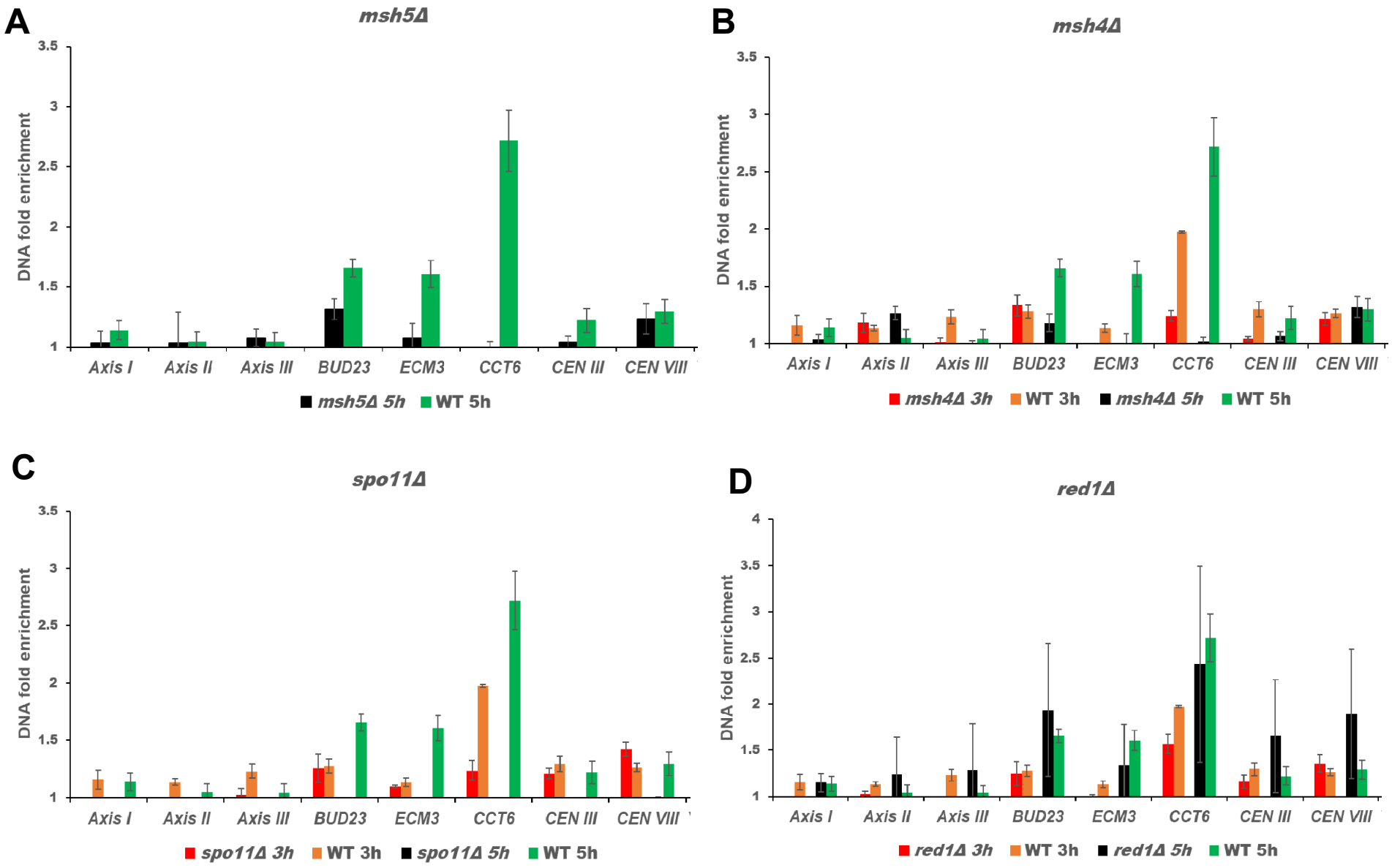
A
msh5Δ
DNA fold enrichment
3.5
3
2.5
2
1.5
1
Axis I
Axis II
Axis III
BUD23
ECM3
CCT6
CEN III
CEN VIII
msh5Δ 5h
WT 5h
B
msh4Δ
DNA fold enrichment
Axis I
Axis II
Axis III
BUD23
ECM3
CCT6
CEN III
CEN VIII
msh4Δ 3h
WT 3h
msh4Δ 5h
WT 5h
C
spo11Δ
DNA fold enrichment
Axis I
Axis II
Axis III
BUD23
ECM3
CCT6
CEN III
CEN VIII
spo11Δ 3h
WT 3h
spo11Δ 5h
WT 5h
D
red1Δ
DNA fold enrichment
4
Axis I
Axis II
Axis III
BUD23
ECM3
CCT6
CEN III
CEN VIII
red1Δ 3h
WT 3h
red1Δ 5h
WT 5h

S5 Fig

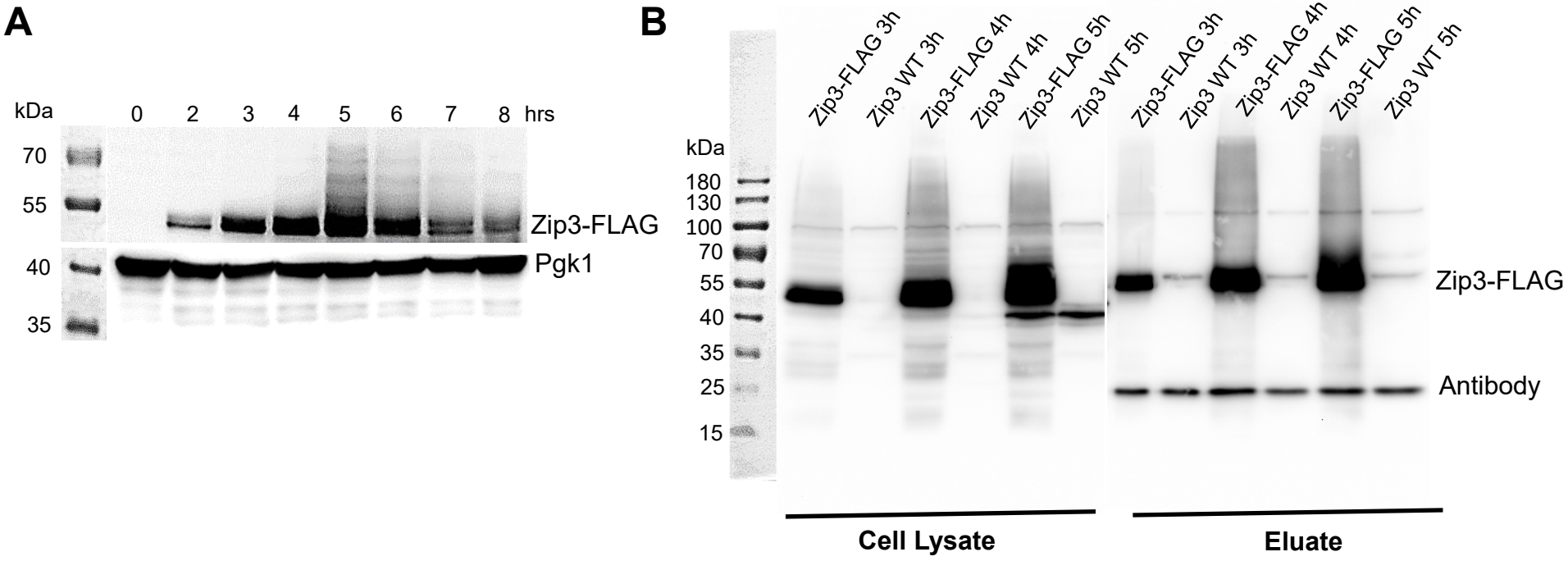
A
kDa
0 2 3 4 5 6 7 8 hrs
70
55
40
35
Zip3-FLAG
Pgk1
B
Zip3-FLAG 3h
Zip3 WT 3h
Zip3-FLAG 4h
Zip3 WT 4h
Zip3-FLAG 5h
Zip3 WT 5h
Zip3-FLAG 3h
Zip3 WT 3h
Zip3-FLAG 4h
Zip3 WT 4h
Zip3-FLAG 5h
Zip3 WT 5h
kDa
180
130
100
70
55
40
35
25
15
Zip3-FLAG
Antibody
Cell Lysate
Eluate

C

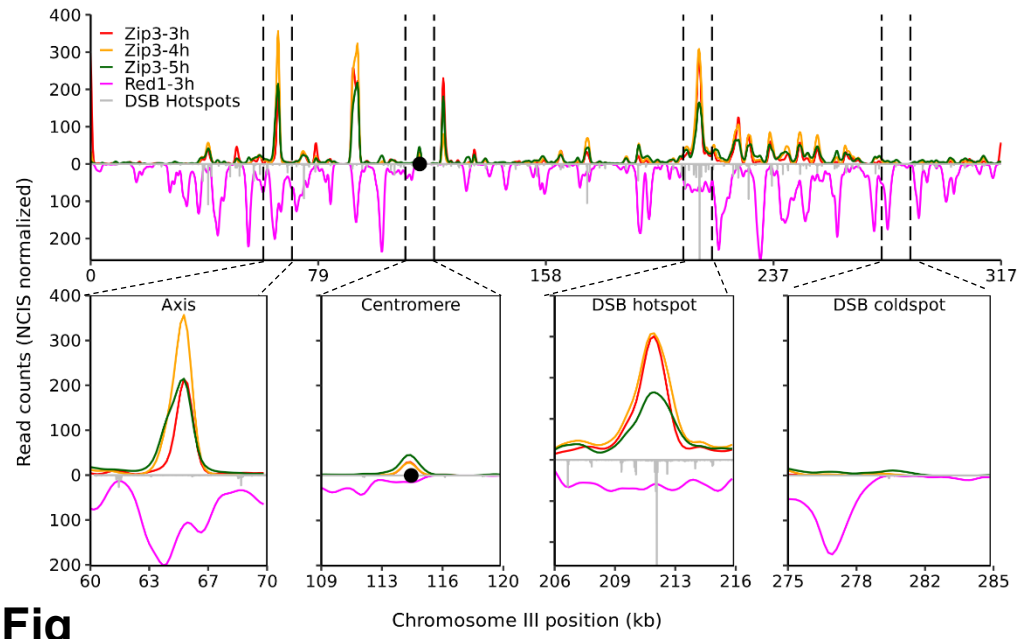
Zip3-3h
Zip3-4h
Zip3-5h
Red1-3h
DSB Hotspots
Read counts (NCIS normalized)
0
79
158
237
317
Axis
Centromere
DSB hotspot
DSB coldspot
Chromosome III position (kb)

S6 Fig

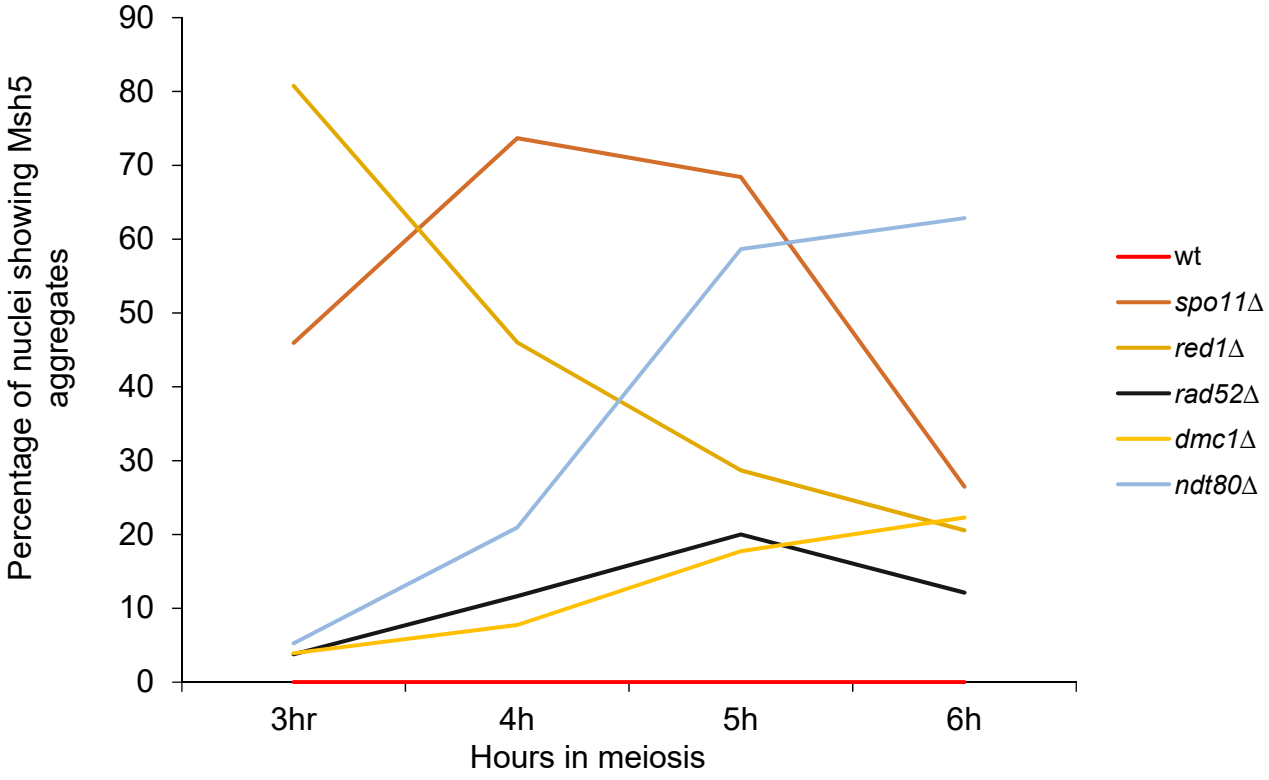
90
80
70
60
50
40
30
20
10
0
Percentage of nuclei showing Msh5 aggregates
3hr
4h
5h
6h
Hours in meiosis
wt
spo11Δ
red1Δ
rad52Δ
dmc1Δ
ndt80Δ

S7 Fig